Emerging hotspots of agricultural drought under climate change

Article

Accepted Version

Black, E. ORCID: https://orcid.org/0000-0003-1344-6186, Wainwright, C. ORCID: https://orcid.org/0000-0002-7311-7846, Allan, R. P. ORCID: https://orcid.org/0000-0003-0264-9447 and Vidale, P. L. ORCID: https://orcid.org/0000-0002-1800-8460 (2026) Emerging hotspots of agricultural drought under climate change. Nature Geoscience. ISSN 1752-0908 doi: 10.1038/s41561-025-01898-8 Available at https://centaur.reading.ac.uk/127637/

To link to this article DOI: http://dx.doi.org/10.1038/s41561-025-01898-8

Publisher: Nature Publishing

Emerging hotspots of agricultural drought under climate change

Emily Black[1,2], Caroline Wainwright[3], Richard P. Allan[1,4] and Pier Luigi Vidale[1,2]

[1]Department of Meteorology, University of Reading, Reading, UK

[2]National Centre for Atmospheric Science, Reading, UK

[3]School of Earth and Environment, University of Leeds, Leeds, UK

[4]National Centre for Earth Observation, Reading, UK

Climate change is intensifying drought risk, yet it is unclear which regions will be most vulnerable in the future. Here, we investigate emerging hotspots of agricultural drought across the tropics and northern hemisphere extra-tropics using climate reanalysis and model simulations under a range of shared socio-economic pathways. Our analysis accounts for soil moisture at growing season onset, as well as for variability during the season itself - linking climate change to the land-surface water balance by classifying the dominant controls on evapotranspiration, including a newly defined state governed by plant extraction of water from the root zone. We show that much of Europe, southern Africa, northern South America, and western North America are emerging hotspots of agricultural drought, with mechanisms of observed drying consistent with future projections. Drought trends are identified even where precipitation projections diverge. By focusing on growing seasons, our approach captures hotspots overlooked by annual metrics and shows that increasing drought frequency is compounded by shifts toward more severe and intense events. These findings have strong implications for food security and highlight the need for drought-resilient adaptation not only in the Global South but also in extratropical regions where risk is already escalating.

Despite the expectation that global precipitation will increase under anthropogenic climate change[1,2], in many regions soil moisture is projected to decline[3] - creating new hotspots of agricultural drought[4-6]. Global analyses of the 6th Coupled Model Intercomparison Project

(CMIP6) ensemble indicate that reductions in soil moisture are projected even in regions where annual precipitation is projected to increase[6,7], and that a climate-change related signal will be detectable before 2060[8]. Soil moisture reflects the local land surface water balance, and hence is affected by precipitation, runoff and the climatic drivers of evaporation (solar radiation, temperature, humidity and wind speed[9,10]), as well as by land-surface and vegetation processes[11]. Variability is thus modulated by land-surface condition and trends in regional climate, which affect evapotranspiration[2,12], interception of precipitation[13] and land-atmosphere coupling[14,15]. On long time scales, warming increases atmospheric water demand[10], leading to increased rates of evapotranspiration[16] and soil moisture decline in terrestrial regions where water is currently plentiful[14,17]. On decadal to centennial timescales, evaporative fluxes are affected by the response of vegetation to CO_2 increase and warming[16,18-20], by changes in winter snow cover[21], and by changes in land use[22].

The complexity of these hydroclimatic interactions has created challenges in disentangling the factors driving regional variation in soil moisture trends[9]. Moreover, although agricultural drought is related to soil moisture deficit, the two are not equivalent. Since most crops are not grown during the whole year, impactful agricultural drought should be defined as root-zone soil moisture deficit during local growing seasons[5] – i.e. the season in which annual crops grow best. Although there has been much work on the land-surface water balance[14], the notion of agricultural drought as a seasonal phenomenon, influenced by both growing season meteorological anomalies, and antecedent conditions, has received limited attention - with most previous studies investigating monthly or annual soil moisture decline[6-8,23]. And yet, the tendency of soil moisture anomalies to persist in time[24-26] means that the risk of seasonal drought is affected by soil moisture levels at season onset, and long-term changes in the land-surface water balance, as well as by variability in precipitation, evpaoration and runoff during the season itself.

Growing seasons differ between the tropics and the extra-tropics (see Methods). In the extra-tropics, where plant growth is controlled by temperature and solar radiation[12], the growing season peaks during the late spring and summer, when solar radiation is highest – i.e. May-September in the northern hemisphere[27]. In the tropics, where seasonal variation in precipitation is more pronounced and solar radiation and temperature are high throughout the year, growing seasons align with local wet seasons (Extended Data Figure 1).

The aim of this study is to identify emerging hotspots of agricultural drought in both the tropics and northern hemisphere extra-tropics. We take a mechanistic approach, focusing on the intersection between climate trends, and the biophysical factors that underpin seasonal variability in the land-surface water balance. We advance on previous work by characterising the drivers of soil moisture variability during locally defined growing seasons - framing the land-surface water balance in terms of spatial and temporal variation in the factors controlling evapotranspiration. This process-based approach enables us to relate global climate model soil moisture projections to the evolving risk of regional agricultural drought - revealing why some regions are rapidly becoming hotspots of agricultural drought whilst others are not.

Evaporative regimes and seasonal cumulation of soil moisture

A conceptual model, used to describe the interplay between climate variability, evaporation and soil moisture, is to define regimes based on the whether actual evapotranspiration (AET) is primarily controlled by energy or water[13,14,17]. Here we extend this framework by identifying a third regime - extraction control - in which seasonal AET variability is governed by plant extraction of water from the root-zone. In this regime, energy and moisture are sufficient for transpiration, so moisture fluxes are determined by demand from plants, rather than by precipitation supply. The extraction-controlled regime thus differs from the energy-controlled regime - for which AET scales with available radiation, and from the water-controlled regime - for which AET co-varies with precipitation and soil-moisture replenishment, and changes in AET can modulate but not reverse the polarity of precipitation-driven changes in soil moisture. Misclassifying extraction control as energy control understates the role of plant regulation in driving variability in seasonal AET, and can exaggerate the effect of increased atmospheric demand on soil moisture drying. Moreover, treating extraction control as water control ties projections of drought to uncertain predictions of precipitation – potentially obscuring robust demand-driven drying signals under warming (see Methods).

The relationships between energy, soil moisture and evapotranspiration illustrated in Figure 1 allow us to classify regions by evaporative regime (see Methods for criteria, and Supplementary Materials for further discussion) – providing a framework for exploring how controls on AET and hence on soil moisture, vary in space and time and differ between models and observations (Figure 2). The contrasting effects of warming on the land-surface water balance in the three regimes are shown in Figure 3, which relates temperature change to seasonal soil-moisture cumulation (i.e. the difference in soil moisture between the beginning and end of the growing season). In the water-controlled regime, AET is driven by precipitation and modulated by warming-induced increase in potential evapotranspiration (PET). The net effect of temperature on AET is thus less clear than in the other regimes – reflecting regional variability in the links between temperature and precipitation trends. The clearest relationship between warming and soil moisture depletion is seen in the energy-controlled regime, with greater warming consistently associated with greater soil moisture decline. For the extraction-controlled regime, the relationship depends on trends in relative humidity (and hence vapour pressure deficit (VPD) – Extended Data Figure 2). In regions where relative humidity is maintained as temperature increases, warming increases the rate of transpiration, and subsequent depletion of soil moisture. In contrast, where relative humidity decreases significantly under warming, reduction in stomatal conductance will reduce transpiration. These competing effects are evident in Figure 3: in the tropical growing seasons, extraction-limited regimes are restricted to coastal areas, where relative humidity is maintained as the atmosphere warms, and consequently warming depletes soil moisture; in contrast, in the northern hemisphere extra-tropical growing seasons and tropical non-growing seasons, relative humidity is projected to decrease strongly in extraction-controlled regions, and greater warming is thus associated with reduced drying (compare Figure 2 with Extended Data Figure 2). In hot regions/seasons (including the tropical dry season), the high temperatures associated with climate change may, furthermore, be sufficient to exceed the optimum temperature – exacerbating this effect[28] (acknowledging that the extent of thermal acclimation to climate change is uncertain and not well-represented by climate models[18]).

Soil moisture memory and trends in drought

At every point on the globe – tropical and extra-tropical - agricultural drought is caused by some combination of low soil moisture at the start of the growing season (antecedent soil moisture) and lower than usual (or more negative than usual) accumulation of soil moisture during the season. Comparison between Figures 4a, b and c confirms that long-term change in growing season soil moisture strongly reflects changing antecedent conditions, rather than changes in seasonal soil moisture accumulation - implying a high degree of soil moisture memory (see also Extended Data Table 1). In this context, soil moisture memory encapsulates the persistence of anomalies over the full range of time scales, from a few months (due to persistence of seasonal antecedent conditions[29]) to decades (reflecting long-term trends in the annual water balance[7]). Our objective in this study is not to analyse spatial variability in decorrelation timescale, but rather to identify which calendar season most strongly explains variability and change in growing-season soil moisture, and whether the dependence on antecedent conditions reflects seasonal persistence or long-term change in the annual water-balance.

In the tropics, where the majority of precipitation occurs during local rainy seasons[30] (Extended Data Figure 1a), on seasonal time scales, soil moisture memory might be expected to be low – with any trace of antecedent conditions obscured by the influx of rainy season precipitation and subsequent cumulation of soil moisture. Extended Data Figure 3 shows that this is true, to an extent, with dry season soil moisture cumulation weakly correlated with wet season soil moisture in arid and semi-arid regions. In humid regions, however, most variance in growing season soil moisture is explained by variability in the preceding dry season. In arid and semi-arid regions, where evaporation is constrained by water availability and hence is positively correlated with precipitation, long term trends in antecedent soil moisture reflect trends in annual precipitation (compare Figure 4c with Extended Data Figure 4b). In more humid regions, where evaporation is energy limited for some or all of the year, over time, increased annual evaporative losses reduce the impact of precipitation increase or exacerbate the impact of precipitation decrease.

For the northern hemisphere extra-tropics, Figure 5a displays the calendar season for which cumulated soil moisture correlates most strongly with growing season soil moisture (the dominant season). The substantial proportion of variance explained by the dominant season (Figure 5b), along with the agreement between the models and ERA5, supports the robustness of this identified season (Extended Data Figure 5). Moreover, the dominant season remains consistent regardless of time series length or whether long-term trends are removed, suggesting that the influence of antecedent conditions reflects seasonal soil moisture memory rather than long-term trends - a conclusion reinforced by the strong explanatory power across time scales (Supplementary Materials Figure S5).

Emerging hotspots of agricultural drought

In the northern hemisphere extra-tropics, soil moisture cumulation during MAM is projected to reduce markedly in all regions, apart from RFE (Russia-Far-East), CNA (Central-North-

America), eastern NWN (N.W.North-America) and GIC (Greenland-Iceland) (Extended Data Figure 6). The reduction results from there being sufficient increases in evapotranspiration to outweigh the effect of observed and projected anthropogenic increases in precipitation[31,32] on cumulated soil moisture (Extended Data Figures 6-8). Figure 5a confirms that MAM is the dominant season, over all of Europe and North America apart from southern central Eurasia (WCA, ECA) and the northern Russian Arctic (RAR). Consistent with these mechanisms, Figure 6 shows that agricultural drought events have been observed to increase in frequency in most Eurasian and some North American SRX regions (NWN, WNA, NEU, WCE, MED, EEU, WSB and ESB) and that the increases are projected to increase over the 21st Century. These findings are consistent with the importance of spring drying in the development of recent severe Eurasian droughts in 2003[33], 2010[34] and 2018[35]. For these reasons, western North America, western Europe and mid-latitude central and eastern Europe (apart from RFE) are identified as emerging drought hotspots (Figure 6a). Notably, these regions align with locations previously identified as exhibiting earlier emergence of severe or intense drought metrics[8,23].

Not all of the northern hemisphere extra-tropics are emerging hotspots of drought. For NEN (North-Eastern North America) and ENA (Eastern North America), although drought is projected to increase in the future, these changes have not been observed in the historical record. In the southern Asian sub-/extra-tropics and in the Caribbean (WCA, ECA, TIB, CAR), the influence of spring soil variability on growing season soil moisture is weaker, and the projected changes in agricultural drought are correspondingly less pronounced and consistent between historical and future periods.

Because tropical precipitation exhibits strong natural interannual variability and because CMIP models underestimate internal climate variability[36], precipitation trends in historical model simulations commonly disagree with observations (compare Supplementary Materials

Figure S3c and d). In semi-arid and arid tropical regions, where agricultural drought is governed by precipitation variability, anthropogenically forced changes may therefore be difficult to detect. In the Horn of Africa, for instance, precipitation droughts have been observed to decrease over the historical period[37,38] (Figure 6g), resulting in a significant increase in the occurrence of agricultural drought (Figure 6f). In the future, however, large anthropogenic increases in precipitation are projected to reduce the incidence of drought (albeit with questions remaining about the reliability of the projections[37,39]). The observed increase in drought in this region cannot, therefore, be classified as an indicator of future change, even though some recent seasonal anomalies have been attributed to anthropogenic forcing[40]. Similarly, in southern South America, recently observed increases in agricultural drought frequency are not projected to persist in the future.

In western southernmost Africa, in contrast, precipitation is observed and projected to decrease – with notable consistency over the CMIP6 ensemble[41]. Because decreased annual precipitation is evident in the future projections; recent drying (including the 2015-2017 'Day Zero drought') has been attributed to climate change[42]; and trends in agricultural drought are driven by consistently projected trends in annual precipitation total (Extended Data Figure 4b), we conclude that western southern Africa (WSAF) is an emerging hot spot of agricultural drought.

In the humid tropics, the situation is analogous to the high latitudes, in that evaporation is controlled by energy in both growing and non-growing seasons (Figure 2). In these regions, warming-induced increases in AET tend to reduce soil moisture – either countering the effect of precipitation increase or amplifying the effect of precipitation decrease. However, not all of the humid tropics can be considered as emerging drought hotspots. In Central Africa (CAF), for example, there remains significant uncertainty in both models and observations of precipitation and soil moisture change – with positive precipitation[43], precipitation-evaporation[44], and streamflow trends[45] in some observations, and in the CMIP6 historical simulations (Supplementary Materials Figure S3), but negative changes in drought events in the ERA5 reanalysis (Figure 6f and g). CAF is therefore not listed as an emerging hotspot of agricultural drought – primarily because of the mismatch between observations of drying and projections of wetting. However, it should be noted because this region is identified as having an energy-controlled evaporation regime, in some regions future decreases in precipitation droughts (Figure 6c) may not translate to reduced soil moisture agricultural drought (Figure 6b). In Amazonia and northern South America (NSA and SAM), in contrast, historical simulations, future projections, and observations agree on signficant worsening of drought incidence and intensity. Indeed, over the last 20 years, in northern South America, there have been four 'once-in-a-hundred-year' events[46], with the effect of El Niño-related rainfall deficits exacerbated by anthropogenic warming[47]. Both NSA and SAM are therefore considered emerging hot spots of agricultural drought.

Wider implications

The results presented here have implications for both mitigation and adaptation policy. Comparison across SSPs indicates that drought incidence is projected to worsen in most of the northern hemisphere extra-tropics under all pathways, but significant increase in the incidence of severe drought is less consistently projected under SSP2-4.5 and SSP1-2.6 than under the more extreme SSP3-7.0 and SSP5-8.5 (Supplementary Materials Figure S6). This finding underlines the societal benefits of reducing emissions.

From an adaptation point of view, Extended Data Figure 9 shows that the projected increase in drought incidence reflects increased drought intensity (consistent with the projected increase in flash drought[48]), and Supplementary Figure 7 indicates that the relative frequency of very severe droughts (|Z-score| > 2) is projected to increase markedly. Crop productivity is disproportionately impacted by intense dry periods - as happened during the 2012 North

American flash drought[49], and by very severe events, such as the 2018 summer drought that affected northern Europe[50]. Our findings thus highlight an urgent need for policy-makers to plan for increased drought stress on crops in Europe and North America (as well as in the more societally vulnerable Global South), and to consider adaptation measures – including introducing drought resistent crop varieties. Because the modelling results presented here do not explicitly consider irrigation, the findings are best interpreted as indicators of increased demand for freshwater for irrigation in heavily irrigated regions – stressing the importance of managing rural water supply in emerging drought hotspots.

To conclude, robust representation of precipitation variability and change remains a challenge for models – but the need to identify regions at increasing risk of agricultural drought is urgent. Moving beyond previous seasonal studies of drought, our study frames global growing seasons in terms of slowly evolving antecedent conditions and trends in soil moisture cumulation during key seasons. By expressing the land-surface water balance in terms of spatially and temporally varying evaporative controls, we identify where soil-moisture decline is robustly projected, and distinguish regions with robust declines from those where change remains uncertain. Advancing on earlier seasonal and annual studies, we identify regions, including western North America, Europe, South America and southern Africa, where recent observed drying is driven by the mechanisms underlying projected worsening of drought and we distinguish such 'emerging hotspots of drought' from regions, such as East Africa and southern South America, where recent observed drying is inconsistent with future projections. Our process-based approach thus clarifies the mechanistic drivers of agricultural drought and robustly identifies emerging hotspots in both the tropics and extra-tropics.

Corresponding author

The corresponding author is Emily Black (e.c.l.black@reading.ac.uk).

Acknowledgements

We acknowledge the following funding: National Centre for Atmospheric Science through the NERC National Capability International Programmes (NC/X006263/1 EB), the EU Horizon Europe programme (Grant No. 101137656, EXPECT EB), National Centre for Earth Observation (NE/RO16518/1 RPA, NE/Y006216/1 RPA).

Author contributions

EB designed the study, carried out the analysis and led the writing. CW provided the code for the objective identification of tropical rainy seasons. RPA and PLV collaborated with EB to frame the conceptual developments. CW, RPA and PLV all commented in detail on the manuscript and contributed to the writing.

Competing interests

The authors decleare no competing interests.

Main paper figures

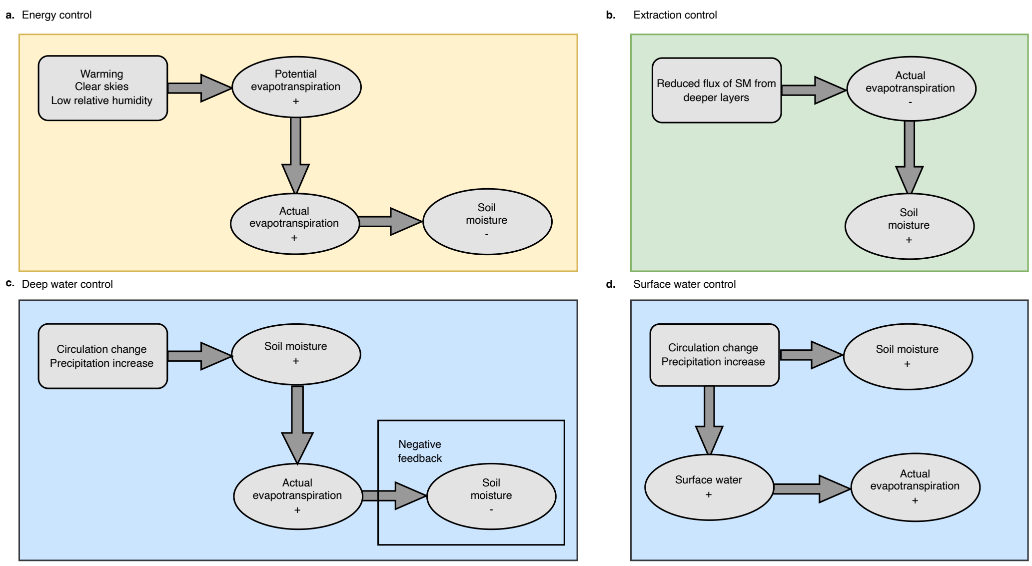

<u>Figure 1: Schematic diagram illustrating the dominant processes for each of the evaporative regimes described in this study</u>. **a. Energy control**: in this regime evaporation is limited by the availability of energy. Actual evapotranspiration (AET) is positively correlated with shortwave radiation flux (SW), and negatively correlated with soil moisture (SM); **b. Extraction control**: in this regime evaporation is limited by the ability of plants to extract water from the soil column. AET and SM are therefore negatively correlated; **c. Deep water control:** in this regime, evaporation is limited by the availability of SM for transpiration. AET is thus positively correlated with SM and the link between SM and AET is directly causal; **d. Surface water control:** in this regime, evaporation is limited by the availability of surface water. AET is thus positively correlated with precipitation, and hence SM, but the link between SM and AET is not directly causal.

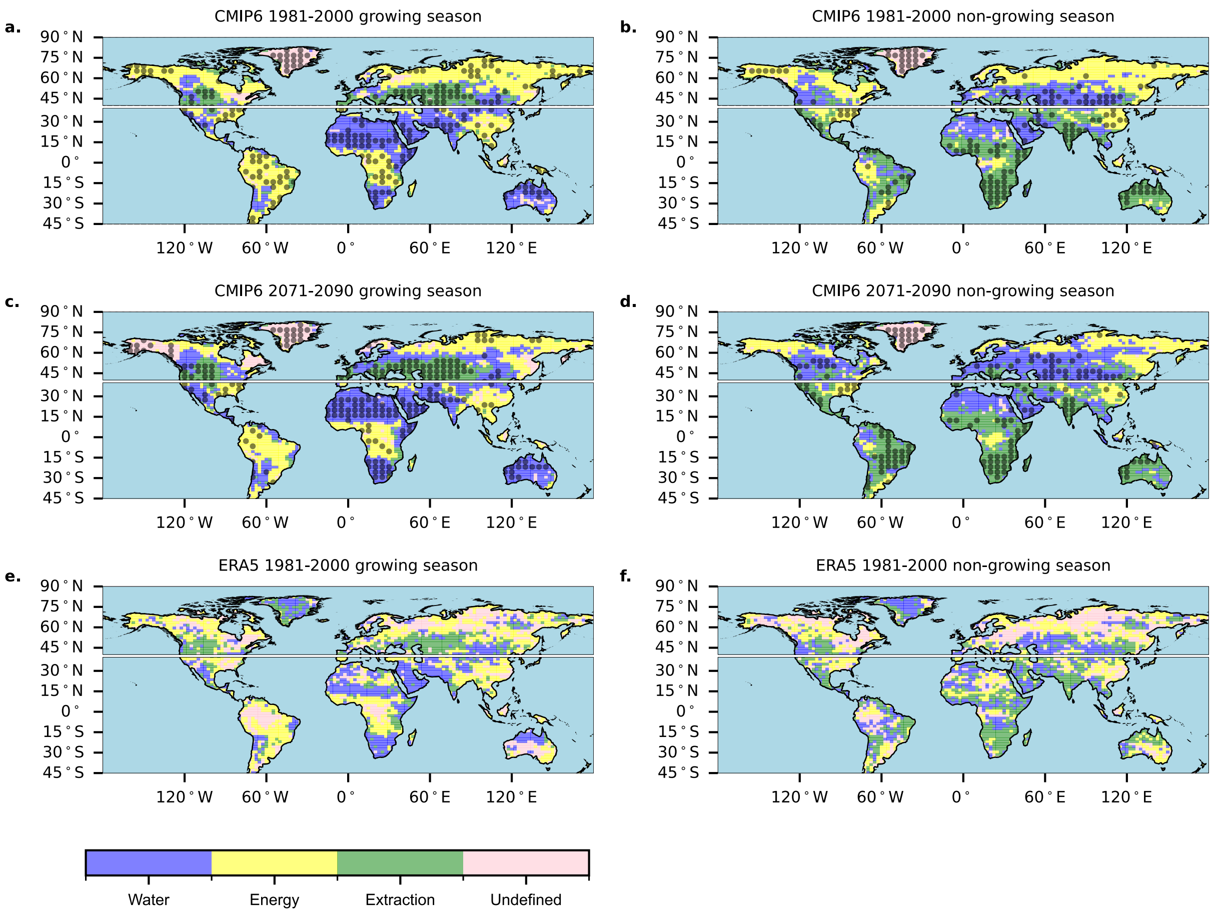

Figure 2: Geographical distribution of evaporative regimes in growing and non-growing seasons. CMIP6 multi-model ensemble for 1981–2000 (a.,b.) and 2071–2090, SSP5-8.5 (c.,d.); ERA5 for 1981–2000 (e.,f.). Left panels show growing seasons (a.,c.,e.); right, non-growing (b.,d.,f.). CMIP6 panels display the multi-model modal regime; circles mark grid cells where ≥67% of models agree on the mode. The maps are split by a horizontal line between the tropics/sub-tropics—where growing seasons coincide with local rains—and the northern-hemisphere extratropics, where growing seasons align with boreal summer (see Methods). Symbols are plotted on alternate grid cells for clarity. [See Suppementary materials Figure S1 for northern hemisphere calendar seasons]

Data sources: The data plotted is derived from CMIP6 data from the ESGF archive and ERA5 from C3S. Basemap: Cartopy/Natural Earth.

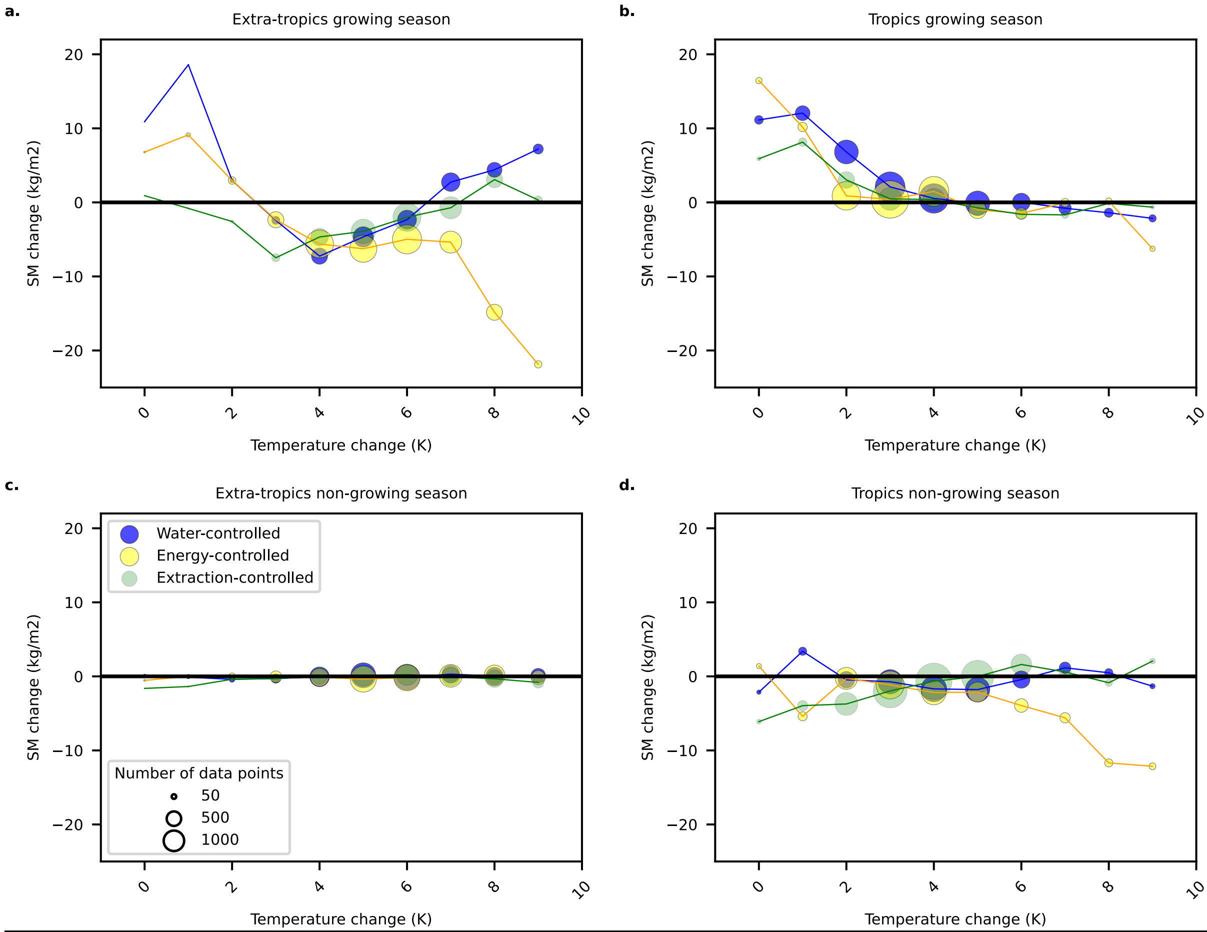

Figure 3: Relationship between seasonally cumulated soil moisture change and warming. The plots compare 2071–2090 (SSP5-8.5; CMIP6 multi-model ensemble), expressed relative to the 1981–2000 baseline for the three evaporative regimes (see colour key). Soil moisture changes are binned according to local temperature change (x-axis shows the lower edge of each bin). The panels show different seasons and latitude ranges: a. extra-tropical northern hemisphere (40^0N-70^0N) growing season; b. tropical (40^0S-40^0N) growing season; c. extra-tropical northern hemisphere non-growing season; d. tropical non-growing season. The size of the circles is scaled by the number of data points in each bin.

Data sources: The data plotted is derived from CMIP6 data from the ESGF archive.

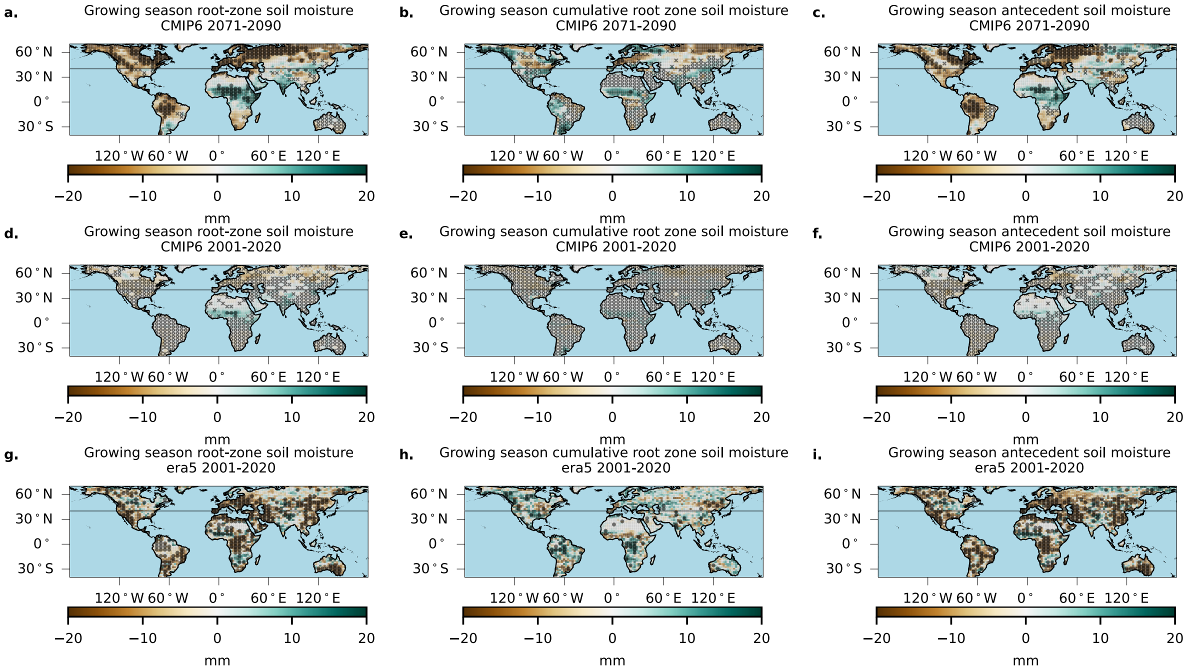

Figure 4: Historical and projected change in root zone soil moisture. CMIP6 multi-model mean 2071–2090 (SSP5-8.5) vs 1981–2000 (a.–c.); CMIP6 multi-model mean 2001–2020 vs 1981–2000 (d.–f.). ERA5: 2001–2020 vs 1981–2000 (g.–i.). Variables: growing-season mean soil moisture (a.,d,g.); cumulated growing-season soil moisture (b.,e.,h.); antecedent (start-of-season snapshot) soil moisture (c.,f.,i.). ERA5 panels (g.-i.): circles denote changes significant at 5% relative to interannual variability. CMIP6 panels (a.-f.): circles indicate ≥67% of models show a significant change of the multi-model mean's polarity at the 5% level; crosses indicate ≥67% agree there is no significant change The maps are split by a horizontal line between the tropics/sub-tropics—where growing seasons coincide with local rains—and the northern-hemisphere extratropics, where growing seasons align with boreal summer (see Methods). Symbols are plotted on alternate grid cells for clarity. [See Supplementary Materials Figure S2 for non-growing season changes; Figure S3 and S4 for growing and non-growing season changes in precipitation and evaporation; Figure S6 additional SSPs].

Data sources: The data plotted is derived from CMIP6 data from the ESGF archive and ERA5 from C3S. Basemap: Cartopy/Natural Earth.

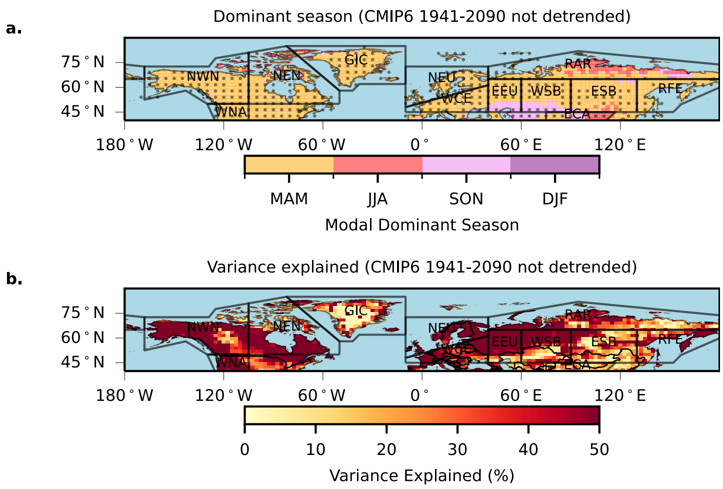

Figure 5: Soil moisture persistence and consequent dominant season in the northern hemisphere extra-tropics a. Calendar season (March-May, June-August, September-November, December-February) for which cumulated soil moisture has the highest positive correlation with growing season (May-September) soil moisture – i.e. the dominant season. Circles indicate points for which at least 67% of models agree on the dominant season; b.) Variance in growing season soil moisture explained by the cumulated soil moisture during the dominant season (grid points where the dominant season is inversely correlated are greyed out). The labelled polygons are regions defined by the IPCC Special Report on Extremes (SRX regions).

Data sources: The data plotted is derived from CMIP6 data from the ESGF archive. Basemap: Cartopy/Natural Earth; Region boundaries: IPCC SREX (licensed via IPCC Atlas repository)

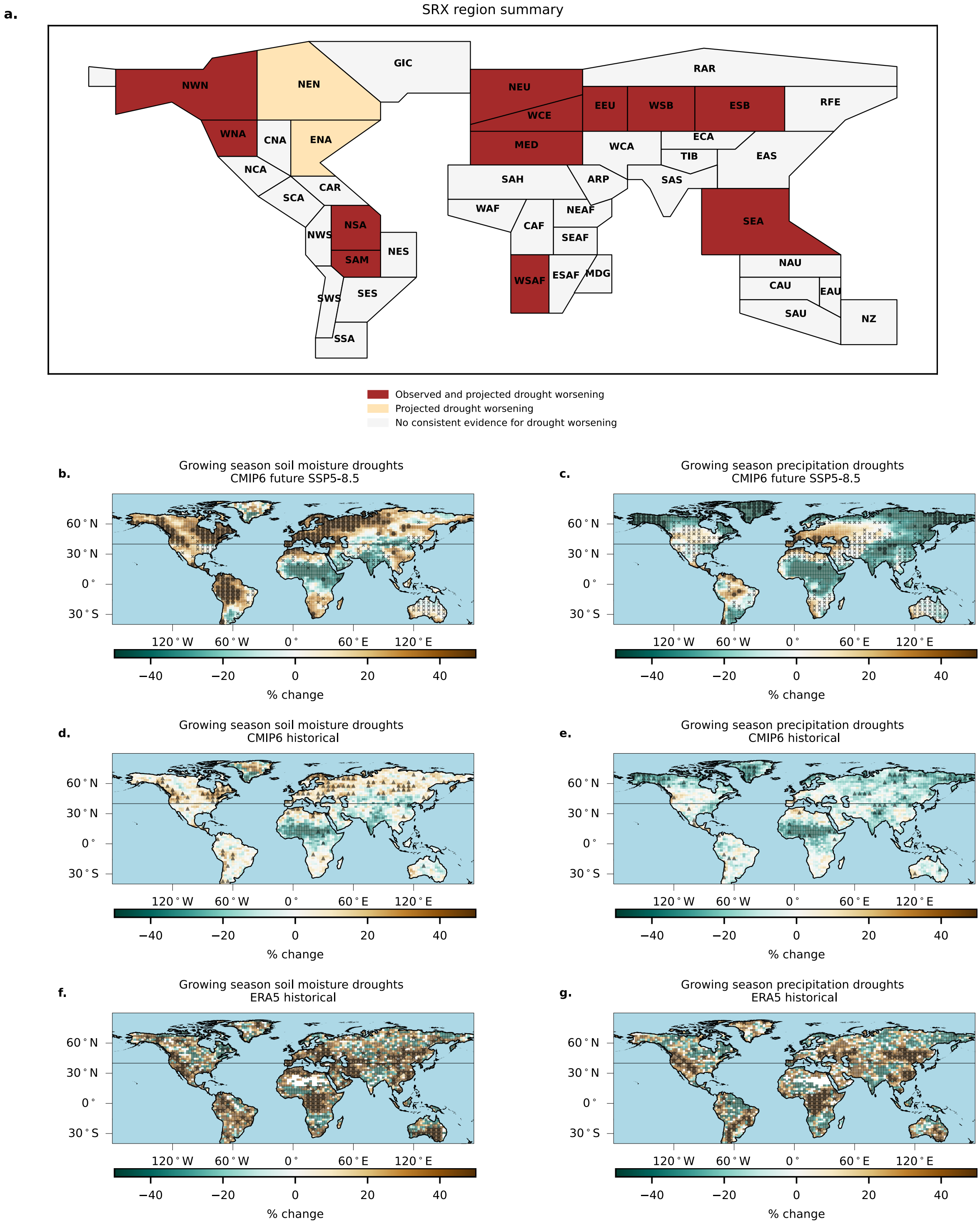

Figure 6: Emerging hotspots of agricultural drought a. SREX regional summary: each region classified as observed and projected increase in soil-moisture-defined drought, projected increase only, or no evidence of worsening (see colour key). b.–c. CMIP6 SSP5-8.5 change in growing-season drought occurrence, 2071–2090 c.f. 1981–2000, for soil moisture events (b.) and precipitation events (c.). d.-e. Historical CMIP6 change, 2001–2020 c.f. 1981–2000,

for soil moisture (D) and precipitation (E). (f.–g.) Historical ERA5 change, 2001–2020 c.f. 1980–2000, for soil moisture events (f.) and precipitation events (g.). For the future projections (b.-c.), circles mark grid cells with 67% of models agreeing on a significant change at the 5% level and crosses indicate that >67% of models agree on no significant change; for the CMIP6 historical trends (d.-e.) triangles mark grid cells where 100% of models agree on the polarity of change; for ERA5 stars indicate significant change (95% level) compared to interannual variablity. For all panels, drought is defined as Z score <-1. The maps are split by a horizontal line between the tropics/sub-tropics—where growing seasons coincide with local rains—and the northern-hemisphere extratropics, where growing seasons align with boreal summer (see Methods). [see Supplementary Materials Figure S7 for additional soil moisture drought thresholds and SSPs]

Data sources: The data plotted is derived from CMIP6 data from the ESGF archive and ERA5 from C3S. Basemap: Cartopy/Natural Earth; Region boundaries: IPCC SRX (licensed via IPCC Atlas repository)

References

1 Allen, M. R. & Ingram, W. J. Constraints on future changes in climate and the hydrologic cycle. *Nature* **419**, 224-232 (2002).

2 Wang, K. & Dickinson, R. E. A review of global terrestrial evapotranspiration: Observation, modeling, climatology, and climatic variability. *Reviews of Geophysics* **50** (2012).

3 Dai, A. Increasing drought under global warming in observations and models. *Nature climate change* **3**, 52-58 (2013).

4 Mishra, A. K. & Singh, V. P. A review of drought concepts. *Journal of hydrology* **391**, 202-216 (2010).

5 Leng, G. & Hall, J. Crop yield sensitivity of global major agricultural countries to droughts and the projected changes in the future. *Science of the Total Environment* **654**, 811-821 (2019).

6 Cook, B. I. *et al.* Twenty-first century drought projections in the CMIP6 forcing scenarios. *Earth's Future* **8**, e2019EF001461 (2020).

7 Lu, J., Carbone, G. J. & Grego, J. M. Uncertainty and hotspots in 21st century projections of agricultural drought from CMIP5 models. *Scientific reports* **9**, 4922 (2019).

8 Joo, J. *et al.* Emergence of significant soil moisture depletion in the near future. *Environmental Research Letters* **15**, 124048 (2020).

9 Vicente-Serrano, S. M. *et al.* Global drought trends and future projections. *Philosophical Transactions of the Royal Society A* **380**, 20210285 (2022).

10 Vicente-Serrano, S. M., McVicar, T. R., Miralles, D. G., Yang, Y. & Tomas-Burguera, M. Unraveling the influence of atmospheric evaporative demand on drought and its response to climate change. *Wiley Interdisciplinary Reviews: Climate Change* **11**, e632 (2020).

11 Berg, A. & Sheffield, J. Climate change and drought: the soil moisture perspective. *Current Climate Change Reports* **4**, 180-191 (2018).

12 Nemani, R. R. *et al.* Climate-driven increases in global terrestrial net primary production from 1982 to 1999. *science* **300**, 1560-1563 (2003).

13 Wang-Erlandsson, L., Van Der Ent, R., Gordon, L. J. & Savenije, H. Contrasting roles of interception and transpiration in the hydrological cycle–Part 1: Temporal characteristics over land. *Earth System Dynamics* **5**, 441-469 (2014).

14 Seneviratne, S. I. *et al.* Investigating soil moisture–climate interactions in a changing climate: A review. *Earth-Science Reviews* **99**, 125-161 (2010).

15 Koster, R. D. *et al.* GLACE: the global land–atmosphere coupling experiment. Part I: overview. *Journal of Hydrometeorology* **7**, 590-610 (2006).

16 Dai, A., Zhao, T. & Chen, J. Climate change and drought: a precipitation and evaporation perspective. *Current Climate Change Reports* **4**, 301-312 (2018).

17 Teuling, A. *et al.* A regional perspective on trends in continental evaporation. *Geophysical Research Letters* **36** (2009).

18 Long, S. Modification of the response of photosynthetic productivity to rising temperature by atmospheric CO2 concentrations: has its importance been underestimated? *Plant, Cell & Environment* **14**, 729-739 (1991).

19 Black, E. *et al.* Cocoa plant productivity in West Africa under climate change: a modelling and experimental study. *Environmental Research Letters* **16**, 014009 (2020).

20 Xu, Z., Jiang, Y. & Zhou, G. Response and adaptation of photosynthesis, respiration, and antioxidant systems to elevated CO2 with environmental stress in plants. *Frontiers in plant science* **6**, 701 (2015).

21 Meira Neto, A. A., Niu, G.-Y., Roy, T., Tyler, S. & Troch, P. A. Interactions between snow cover and evaporation lead to higher sensitivity of streamflow to temperature. *Communications Earth & Environment* **1**, 56 (2020).

22 te Wierik, S. A., Cammeraat, E. L., Gupta, J. & Artzy-Randrup, Y. A. Reviewing the impact of land use and land-use change on moisture recycling and precipitation patterns. *Water Resources Research* **57**, e2020WR029234 (2021).

23 Chen, S. & Yuan, X. The Timing of Detectable Increases in Seasonal Soil Moisture Droughts Under Future Climate Change. *Earth's Future* **12**, e2023EF004174 (2024).

24 Koster, R. D. & Suarez, M. J. Soil moisture memory in climate models. *Journal of hydrometeorology* **2**, 558-570 (2001).

25 Orth, R. & Seneviratne, S. I. Predictability of soil moisture and streamflow on subseasonal timescales: A case study. *Journal of Geophysical Research: Atmospheres* **118**, 10,963-910,979 (2013).

26 Seneviratne, S. I. & Koster, R. D. A revised framework for analyzing soil moisture memory in climate data: Derivation and interpretation. *Journal of Hydrometeorology* **13**, 404-412 (2012).

27 Myoung, B., Choi, Y. S., Hong, S. & Park, S. K. Inter-and intra-annual variability of vegetation in the northern hemisphere and its association with precursory meteorological factors. *Global Biogeochemical Cycles* **27**, 31-42 (2013).

28 Black, E. *et al.* Cultivating C4 crops in a changing climate: sugarcane in Ghana. *Environmental Research Letters* **7** (2012). https://doi.org/10.1088/1748-9326/7/4/044027

29 Esit, M. *et al.* Seasonal to multi-year soil moisture drought forecasting. *npj Climate and Atmospheric Science* **4**, 16 (2021).

30 Dunning, C. M., Black, E. C. & Allan, R. P. The onset and cessation of seasonal rainfall over Africa. *Journal of Geophysical Research: Atmospheres* **121**, 11,405-411,424 (2016).

31 Balan Sarojini, B., Stott, P. A. & Black, E. Detection and attribution of human influence on regional precipitation. *Nature Climate Change* **6**, 669-675 (2016). https://doi.org/10.1038/nclimate2976

32 Balan Sarojini, B., Stott, P. A., Black, E. & Polson, D. Fingerprints of changes in annual and seasonal precipitation from CMIP5 models over land and ocean. *Geophysical Research Letters* **39** (2012). https://doi.org/10.1029/2012gl053373

33 Black, E., Blackburn, M., Harrison, R. G., Hoskins, B. J. & Methven, J. Factors contributing to the summer 2003 European heatwave. *Weather* **59**, 217-223 (2004). https://doi.org/10.1256/wea.74.04

34 Miralles, D. G., Teuling, A. J., Van Heerwaarden, C. C. & Vilà-Guerau de Arellano, J. Mega-heatwave temperatures due to combined soil desiccation and atmospheric heat accumulation. *Nature geoscience* **7**, 345-349 (2014).

35 Bakke, S. J., Ionita, M. & Tallaksen, L. M. The 2018 northern European hydrological drought and its drivers in a historical perspective. *Hydrology and Earth System Sciences* **24**, 5621-5653 (2020).

36 Ahn, M.-S., Gleckler, P. J., Lee, J., Pendergrass, A. G. & Jakob, C. Benchmarking simulated precipitation variability amplitude across time scales. *Journal of Climate* **35**, 6773-6796 (2022).

37 Wainwright, C. M. *et al.* 'Eastern African paradox' rainfall decline due to shorter not less intense long rains. *npj Climate and Atmospheric Science* **2** (2019). https://doi.org/10.1038/s41612-019-0091-7

38 Lyon, B. & DeWitt, D. G. A recent and abrupt decline in the East African long rains. *Geophysical Research Letters* **39** (2012).

39 Tierney, J. E., Ummenhofer, C. C. & Demenocal, P. B. Past and future rainfall in the Horn of Africa. *Science advances* **1**, e1500682 (2015).

40 Lott, F. C., Christidis, N. & Stott, P. A. Can the 2011 East African drought be attributed to human-induced climate change? *Geophysical Research Letters* **40**, 1177-1181 (2013).

41 Almazroui, M. *et al.* Projected change in temperature and precipitation over Africa from CMIP6. *Earth Systems and Environment* **4**, 455-475 (2020).

42 Pascale, S., Kapnick, S. B., Delworth, T. L. & Cooke, W. F. Increasing risk of another Cape Town "Day Zero" drought in the 21st century. *Proceedings of the National Academy of Sciences* **117**, 29495-29503 (2020).

43 Maidment, R. I., Allan, R. P. & Black, E. Recent observed and simulated changes in precipitation over Africa. *Geophysical Research Letters* **42**, 8155-8164 (2015). https://doi.org/10.1002/2015gl065765

44 Allan, R. P. Amplified seasonal range in precipitation minus evaporation. *Environmental Research Letters* **18**, 094004 (2023).

45 Müller, O. V., McGuire, P. C., Vidale, P. L. & Hawkins, E. River flow in the near future: a global perspective in the context of a high-emission climate change scenario. *Hydrology and Earth System Sciences* **28**, 2179-2201 (2024).

46 Marengo, J. A. *et al.* The drought of Amazonia in 2023-2024. *American Journal of Climate Change* **13**, 567-597 (2024).

47 Clarke, B. *et al.* Climate change, not El Niño, main driver of exceptional drought in highly vulnerable Amazon River Basin. *Grantham Institute for Climate Change* **143** (2024).

48 Black, E. Global change in agricultural flash drought over the 21st century. *Advances in Atmospheric Sciences* **41**, 209-220 (2024). https://doi.org/10.1007/s00376-023-2366-5

49 Otkin, J. A. *et al.* Flash droughts: A review and assessment of the challenges imposed by rapid-onset droughts in the United States. *Bulletin of the American Meteorological Society* **99**, 911-919 (2018).

50 Blauhut, V. *et al.* Lessons from the 2018–2019 European droughts: a collective need for unifying drought risk management. *Natural hazards and earth system sciences* **22**, 2201-2217 (2022).

Methods

Models and data used

For this study, an ensemble of 17 models from the 6th Coupled Model Intercomparison Project (CMIP6[51]) was analysed (Supplementary Materials Table 1). The first ensemble member was used from each model. The models selected encompass a wide variety of land surface models, resolutions and soil thicknesses. The primary selection criterion for the was the availability of all required variables for the historical period and the SSP5-8.5 pathway (a smaller subset of models was used for the plots of other SSP pathways: SSP1-2.6, SSP3-7.0, SSP2-4.5).

The required variables were:

- pr (precipitation)
- mrsol (soil moisture in soil layers)
- evspsbl (surface evapotranspiration)
- tas (near surface air temperature)
- hurs (surface relative humidity)
- rsds (surface flux of shortwave radiation)

The CMIP6 data were analysed for the historical simulations (starting at 1940), spliced together with SSP5-8.5, SSP1-2.6, SSP3-7.0, SSP2-4 output for 2015-2100. As an observation-based benchmark we use ERA5 reanalysis[52] selected for its global coverage, variable completeness and internal physical consistency at daily resolution, and documented skill in capturing soil-drying and related hydroclimate variability[53].

Data downloaded at monthly resolution, and then interpolated to pentadal resolution for separation into wet and dry seasons (see next section). Using monthly, rather than daily data, greatly reduced computational cost and allowed us to use a larger model ensemble. All data were re-gridded to a common 144x96 horizontal grid (using bi-linear interpolation).

Identification of growing seasons

For the purposes of identifying growing seasons, data were split by latitude into 40^0S - 40^0N and 40^0N - 90^0N. In the main text, these regions were referred to informally as the ‘tropics’ and the ‘northern hemisphere extra tropics’. For the northern hemisphere extra tropics, the growing season was defined everywhere as May 1^{st} – September 30^{th} (referred to informally as northern hemisphere or boreal summer), with the rest of the year referred to as northern hemisphere winter.

For the tropics, it is assumed that growing seasons align with local wet seasons. We acknowledge that crop-specific shifts in planting or phenology under heat stress are important but require a separate, phenology-resolved framework and are therefore beyond the scope of this hydroclimate-focused analysis. We define wet/dry seasons using precipitation thresholds to reflect rainy season water supply and to enable consistent model–reanalysis comparisons. Because the timing of tropical wet seasons varies considerably from one region to another, local growing seasons were identified using a well-established objective method for identifying rainy season start and end date[30,54]. The method identifies the start and end of the rainfall season based on cumulative rainfall anomalies. It first computes sub-monthly rainfall anomalies relative to the annual mean. Then, a cumulative sum of these anomalies is calculated, forming a curve that typically shows a minimum near the season start and a maximum near the season end. The start date is the time when this cumulative anomaly reaches its lowest point, indicating the transition from the dry to the wet season. The end date is when the cumulative anomaly reaches its highest point, marking the return to drier conditions.

In this paper, the following adjustments/simplifications were made:

- the method has been adapted to be applied to monthly data, interpolated to pentadal scale
- no attempt is made to remove humid regions or regions with weak precipitation seasonality

- for regions with two seasons, the algorithm picks out the main rainy season. It should be noted that only a few regions experience two rainy seasons, including East Africa, part of Pakistan and a few grid points in northern Brazil (see Figure 1 in Wainwright et al. 2021[55]). For the purposes of this study, the main rainy season was considered the growing season and periods outside the primary rainy season were treated as the 'dry season' or the 'non-growing season'

The local growing seasons were defined individually for each model or reanalysis, which means that when calculating the growing season mean for the multi-model ensemble, different dates were included for each model (see Supplementary Materials Figure S15a and b for maps of the multi-model mean start and end rainy season dates). Furthermore, because rainy season timing exhibits significant trends[55], the algorithm was implemented for a running 10-year window. There is some variation in precipitation seasonality amongst climate models (Supplementary materials Figure S15c and d). For this reason, season timings were derived separately for each model, meaning that the wet seasons identified were specific to the model in question. For calculation of multi-model means, the individual model wet/dry seasons were averaged.

The differences between projected growing season soil moisture (Figure 4A) and annual soil moisture change (Extended Data Figure 4D) underline the importance of treating agricultural drought as a growing season phenomenon. In some regions – especially in the northern hemisphere extra-tropics, equating changes in agricultural drought to changes in annual soil moisture underplays the projected increased risk of drought. In central and eastern Europe, for instance, projected changes in annual soil moisture are small and inconsistent between models, while growing season soil moisture is projected to decrease strongly – leading to increased incidence of drought. In North America, annual soil moisture depletion is concentrated in eastern regions, but projected increase of agricultural drought frequency is most marked in the west (consistent with historically observed trends). These discrepancies explain the differences between the conclusions of this study and previous assessments of change in global soil moisture, which focused on annual metrics and thus did not highlight western North America or central Europe as regions of severe projected decline in soil moisture[7,56].

Evaporative regimes: Further details of methodologies

To identify regimes, we use the following variables: soil moisture [seasonally cumulated soil moisture interpolated to 1m depth (based on CMIP6 variable *mrsol*)], AET [total actual evapotranspiration (CMIP6 variable *evspsbl*] and SW [short wave radiation flux at the surface (CMIP6 variable *rsds*)]. A key point is that regimes are determined based on time series of rootzone soil moisture cumulation (i.e. the difference between the soil moisture at season end and beginning), rather than on absolute values. Using cumulation allows us to look at the seasonal land-surface water balance independently of soil moisture persistence.

The criteria for each regime is as follows:

Energy control: negative interannual correlation (<-0.1) between AET and soil moisture and positive correlation (>0.1) between AET and SW

Surface/Deep Water control: positive interannual correlation (>0.1) between AET and soil moisture; and weak or negative correlation (<0.1) between AET and SW.

Extraction control: negative interannual correlation (<-0.1) between AET soil moisture, and weak or negative correlation (<0.1) between AET and SW (rsds)

Points that did not meet the criteria to be assigned to an evaporative regime were denoted as 'Undefined'. The correlations were calculated for interannual variability for individual seasons as shown on Figure 2 and Supplementary Materials Figure S1.

Drought metrics

The following drought metrics are investigated:

- Drought occurrence is defined as the number of events where the mean growing season soil moisture at a grid point is lower than a specified threshold, with the threshold defined in terms of the number of standard deviations from the mean (Z-score). Figure 6 uses a threshold of 1 standard deviation from the mean – with additional thresholds given in supplementary information (Supplementary materials Figure S7)
- Change in drought intensity is defined as the percentage change in minimum soil moisture (expressed in terms of Z-score)
- Change in drought duration is defined as the percentage change in a dry spell index: the number of pentads that fall within a continuous sequence of at least 12 dry pentads (2 months), with a dry pentad defined as having a z-score < -0.5.

To ensure enough events for meaningful statistical testing (see section on statistical testing below for further details), rather than using 20-year historical and future time slices, the metrics are compared for 1941-2020 and 2021-2100. In addition, the criteria for defining a drought is relaxed to seasonal soil moisture z-score anomalies <-0.5.

Further details of analysis of statistical testing

All hypothesis tests are conducted pixelwise and model-by-model on annual/seasonal time-slice series, and significance is then summarized across models via a consensus rule: multi-model maps display stippling only where ≥67% of models are individually significant and agree in sign with the multi-model mean. The ≥67% threshold follows the 'majority agreement' convention used in multi-model assessments (e.g., IPCC AR6 uses ≈66% for majority agreement).

When interpreting multi-model means, we therefore classify results as:

- Robust detection of a signal of change: >67% of models indicate a statistically significant change (per the variable-appropriate tests above) with the same polarity as the multi-model mean.
- Robust detection of no signal of change: >67% of models indicate no statistically significant change.
- Indeterminate: the criteria above are not met (models disagree on polarity and/or significance).

Given strong spatial correlation and many simultaneous tests, we do not apply pixelwise multiple-testing corrections; instead, we require cross-model agreement (≥67% with common sign) before highlighting a change. This consensus threshold suppresses isolated false positives that arise from multiplicity while highlighting signals that are reproducible across models.

We select the test to match the distribution and dependence structure of each variable. For drought metrics (minimum growing-season soil moisture and dry-spell indices), which are bounded, skewed or discrete, we use a rotation (circular-shift) permutation that preserves year-to-year dependence and seasonality while testing the mean shift without distributional assumptions. For event counts (proportion of event years per slice), we use a two-proportion score test with effective sample size (prop_neff) that inflates the standard error using each slice's AR(1). For continuous seasonal/annual aggregates (e.g., precipitation, temperature, moisture indices), we apply Welch's unequal-variance t-test after within-slice detrending, and we verify assumptions by mapping lag-1 autocorrelation and D'Agostino–Pearson K^2 on AR(1)-whitened residuals.

<u>Event-count comparisons (two-sample proportions with dependence).</u>

For windowed counts of drought events (yearly indicators aggregated over a time slice), we compare the proportion of event years between periods using a two-proportion score test with effective sample size to account for autocorrelation.

Let x_k be the number of event years and n_k the number of years in period $k \in [1,2]$. The estimator $\hat{p}_k = x_k/n_k$ remains unbiased under weak serial dependence, but its variance is inflated. We estimate each slice's lag-1 autocorrelation $\hat{\rho}_{1,k}$ from the binary event series and form

$$n_{k,\mathrm{eff}} = n_k \frac{1-\hat{\rho}_{1,k}}{1+\hat{\rho}_{1,k}},$$

clipped to $[2, n_k]$. We then test $H_0: p_1 = p_2$ using the score (z) test for two proportions with the standard errors computed using $n_{k,\mathrm{eff}}$:

$$\widehat{\mathrm{SE}}^2(\hat{p}_1 - \hat{p}_2) = \frac{\hat{p}(1-\hat{p})}{n_{1,\mathrm{eff}}} + \frac{\hat{p}(1-\hat{p})}{n_{2,\mathrm{eff}}}, \hat{p} = \frac{x_1 + x_2}{n_1 + n_2}.$$

<u>Drought-metric comparisons (rotation permutation with temporal dependence preserved).</u> For drought metrics that may be non-Gaussian and bounded, including minimum growing-season soil moisture and our dry-spell index - we compare periods using a circular-shift permutation test that maintains the observed serial structure:

Let y_t denote the annual metric for year $t = 1, \dots, N$, spanning two contiguous time slices W_1(baseline) and W_2(comparison). The observed test statistic is the difference in window means, $\Delta_{\mathrm{obs}} = \bar{y}_{W_2} - \bar{y}_{W_1}$(reported with its sign). Under the null of no change in the mean across windows, years are exchangeable up to a rotation that preserves autocorrelation and seasonality. We therefore generate B cyclic shifts: for shift $s \in [0, \dots, N-1]$, form $y_t^{(s)} = y_{(t+s \bmod N)}$, recompute $\Delta^{(s)}$, and obtain a two-sided p-value

$$p = \frac{1 + [\ |\Delta^{(s)}| \geq |\Delta_{\mathrm{obs}}|\ ]}{1+B},$$

This construction exactly preserves each series' empirical distribution and interannual dependence, while testing only the shift in the mean between slices.

<u>Continuous seasonal/annual fields (Welch's unequal-variance t-test with dependence/normality checks).</u>

For continuous-valued aggregates (e.g., seasonal/annual means of precipitation, temperature, and moisture indices), we test for differences between 20-yr slices using Welch's t-test on period means, allowing unequal variances across slices. Let $\bar{x}_k$ and s_k^2 be the mean and variance of slice $k \in \{1,2]$ with n_k years. The test statistic is

$$T = \frac{\bar{x}_2 - \bar{x}_1}{\sqrt{s_1^2/n_1 + s_2^2/n_2}},$$

Because these fields are seasonal/annual aggregates formed from many pentads/days, their sampling distributions are close to normal by a central-limit effect; nevertheless we verify assumptions at each grid cell and model by (i) estimating lag-1 autocorrelation of the detrended series (R^2 typically << 0.1), and (ii) quantifying normality using the D'Agostino–Pearson K^2 diagnostic on AR(1)-whitened residuals (low K^2 and non-significant p-values over all regions apart from the hyper-arid Sahara and Arabian peninsula). Example plots of these diagnostics are shown in Supplementary Materials Figure S16.

Data availability statement

All input data used in this study are publicly available. Climate model simulations were obtained from the Earth System Grid Federation (ESGF) CMIP6 archive (historical and ScenarioMIP runs; models listed in Table 1). Reanalysis data were taken from the ERA5 dataset, available through the Copernicus Climate Data Store. The figures include basemap data from Cartopy and region boundary data from the IPCC-WGI Atlas repository[57].

All intermediate datasets used to produce the figures can be reproduced from these public sources using the code released with this paper and can be downloaded via Zenodo (DOI: 10.5281/zenodo.17752786).

Code availability statement

The code required to create all the figures included in this paper and to produce the data files from the sources listed above is available via Zenodo (DOI: 10.5281/zenodo.17705187.)

Methods only references

51 O'Neill, B. C. *et al.* The scenario model intercomparison project (ScenarioMIP) for CMIP6. *Geoscientific Model Development* **9**, 3461-3482 (2016).

52 Hersbach, H. *et al.* The ERA5 global reanalysis. *Quarterly Journal of the Royal Meteorological Society* **146**, 1999-2049 (2020).

53 Hirschi, M., Stradiotti, P., Crezee, B., Dorigo, W. & Seneviratne, S. I. Potential of long-term satellite observations and reanalysis products for characterising soil drying: trends and drought events. *Hydrology and Earth System Sciences* **29**, 397-425 (2025).

54 Liebmann, B. *et al.* Seasonality of African precipitation from 1996 to 2009. *Journal of Climate* **25**, 4304-4322 (2012).

55 Wainwright, C. M., Black, E. & Allan, R. P. Future changes in wet and dry season characteristics in CMIP5 and CMIP6 simulations. *Journal of Hydrometeorology* **22**, 2339-2357 (2021). https://doi.org/10.1175/jhm-d-21-0017.1

56 Berg, A., Sheffield, J. & Milly, P. C. Divergent surface and total soil moisture projections under global warming. *Geophysical Research Letters* **44**, 236-244 (2017).

57 Iturbide, M. *et al.* Implementation of FAIR principles in the IPCC: the WGI AR6 Atlas repository. *Scientific Data* **9**, 629 (2022).

Extended Data

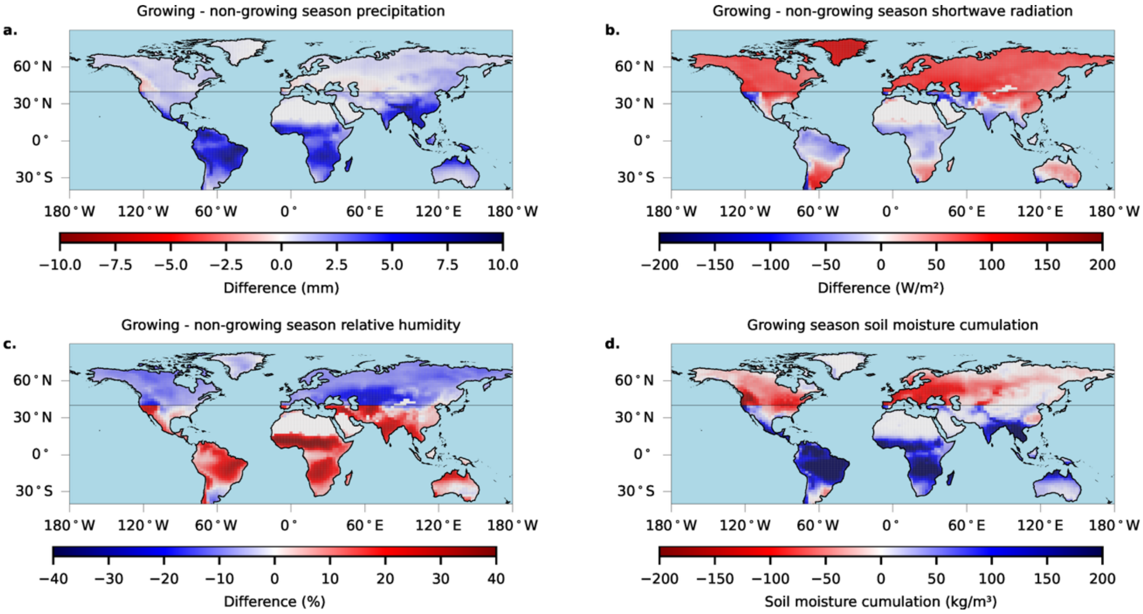

Extended Data Figure 1: Difference between growing season and non-growing season A) precipitation rate; B) potential evapotranspiration (PET); and C) shortwave radiation flux (SW); Panel D shows the soil moisture cumulated during the growing season. All panels show the CMIP6 multi-model mean, for the period 1980-2000.

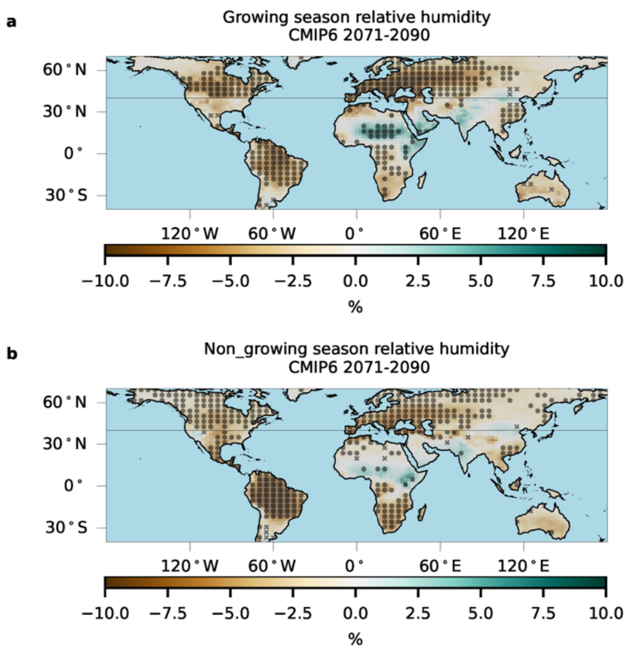

Extended data figure 2: Projected changes in relative humidity under an SSP5-8.5 scenario for 2071-2090 compared to a baseline of 1981-2000

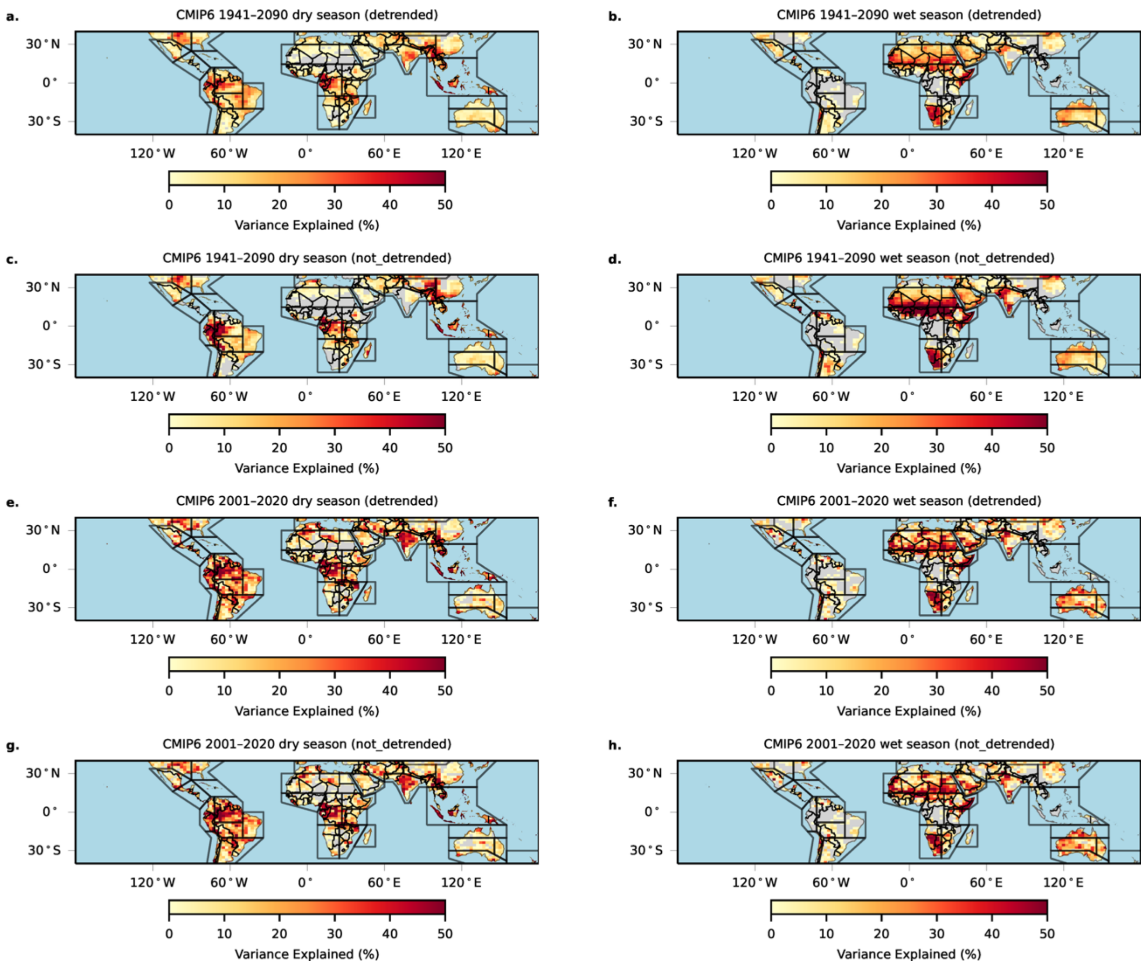

Extended Data Figure 3: Proportion of wet season total soil moisture variance explained by cumulated soil moisture during the dry season (panels A, C, E); and the wet season (panels B, D, F) for the CMIP6 multi-model mean for 1940-2090, with no detrending (panels A and B); ERA5 reanalysis for 2000-2020 with linear detrending applied to both variables (panels C and D); and the ERA5 reanalysis for 2000-2020 with linear detrending applied to both variables (panels E and F). Regions with a negative Pearson correlation coefficient between the two variables are greyed out. The regions shown are the SRX regions referred to in the main paper.

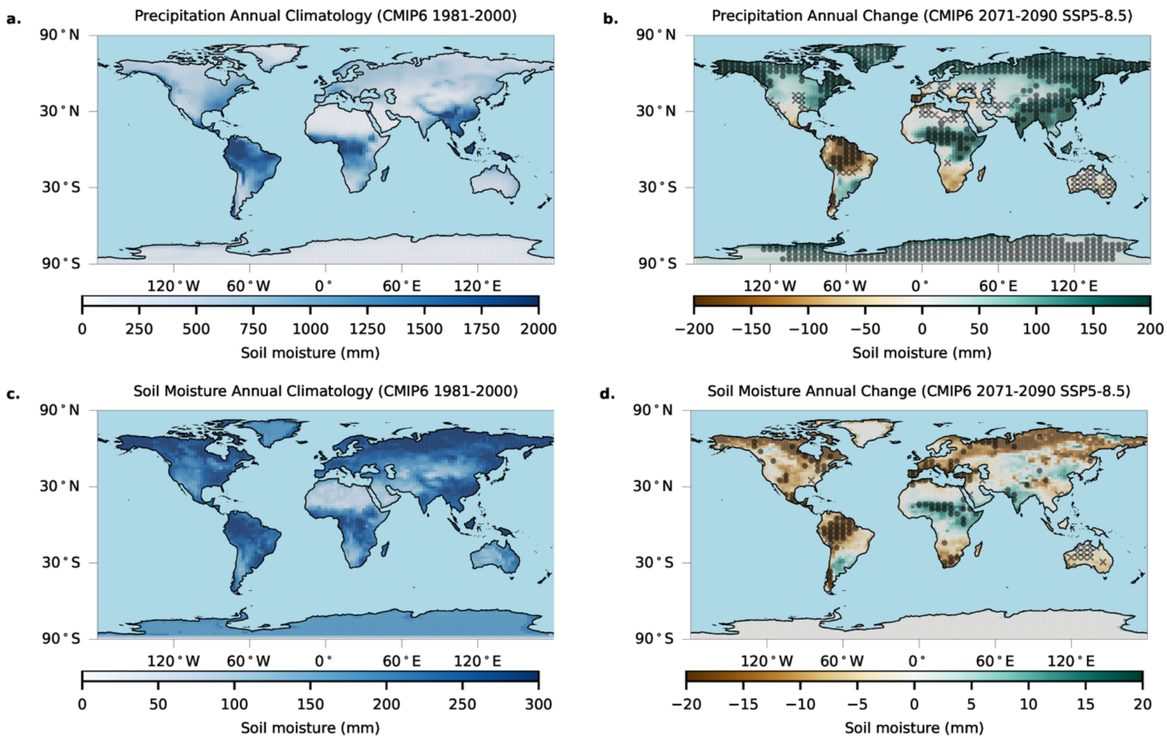

Extended data figure 4: Historical and projected changes in annual precipitation and soil moisture. (A) Multi-model mean annual precipitation climatology (1980–2000). (B) Projected precipitation change, 2070–2090 vs 1980–2000 (SSP5-8.5). (C) Multi-model mean annual 1 m soil-moisture climatology (1980–2000). (D) Projected soil-moisture change, 2070–2090 vs 1980–2000 (SSP5-8.5). Circles mark grid cells where ≥67% of models show a significant change with the MMM's polarity; crosses mark ≥67% agreement on no significant change (5% level). Markers are plotted on alternate grid points for clarity.

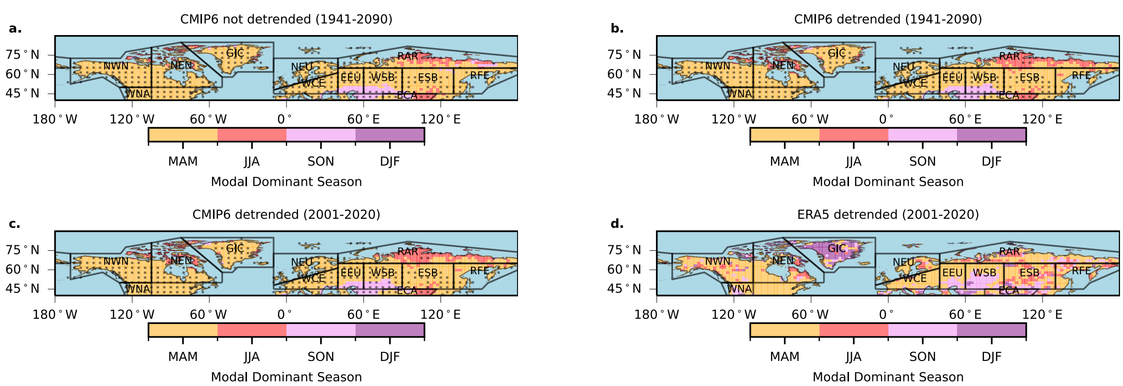

Extended data figure 5: Dominant season for (A) the CMIP6 multi-model model ensemble (1941-2090 not detrended); (B) ERA5 reanalysis (2000-2020 detrended); C) the CMIP6 multi-model mode (2000-2020 detrended). Grid points with >67% of models agreeing on the modal dominant season are indicated with a filled circle.

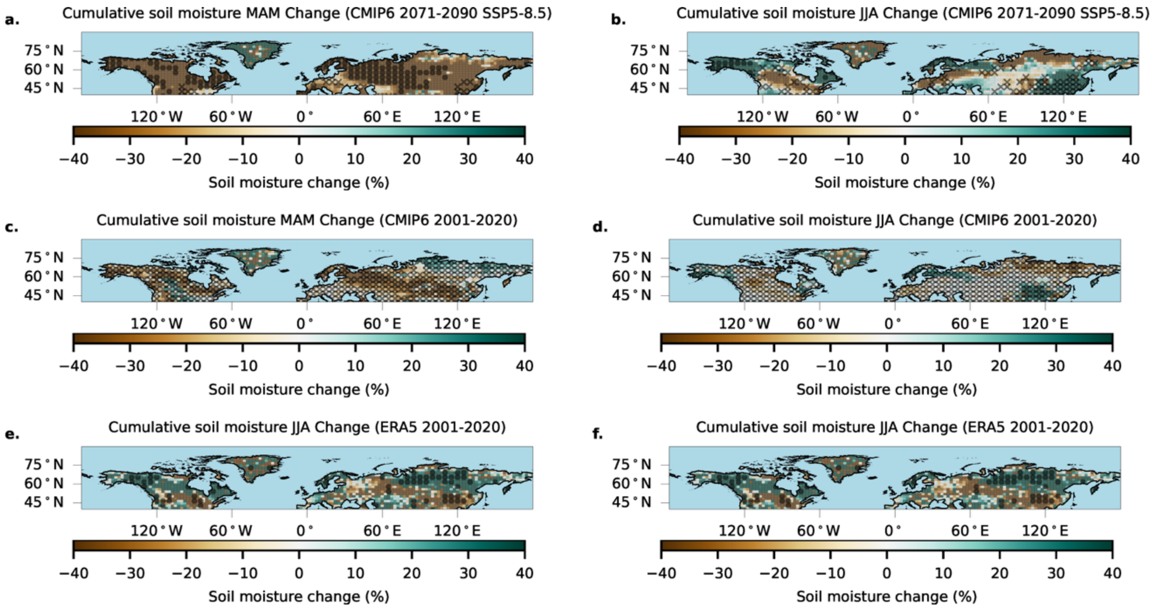

Extended data figure 6: Observed and projected percentage change in cumulated soil moisture in the northern hemisphere extra-tropics for the MAM and JJA calendar seasons (all changes are relative to 1981-2000). Top row (panels A and B): CMIP6 multi-model ensemble 2071-2090 time slice; middle row (panels C and D) CMIP6 multi-model ensemble 2001-2020 time slice; bottom row (panels E and F) ERA5 2001-2020 time slice. For the CMIP6 plots, circles indicate that at least 67% of the models display a significant change of the same polarity as the multi-model mean; crosses indicate that at least 67% of models agree that there is no significant change at the 95% level. [Additional scenarios shown in Supplementary Information Figure S10]

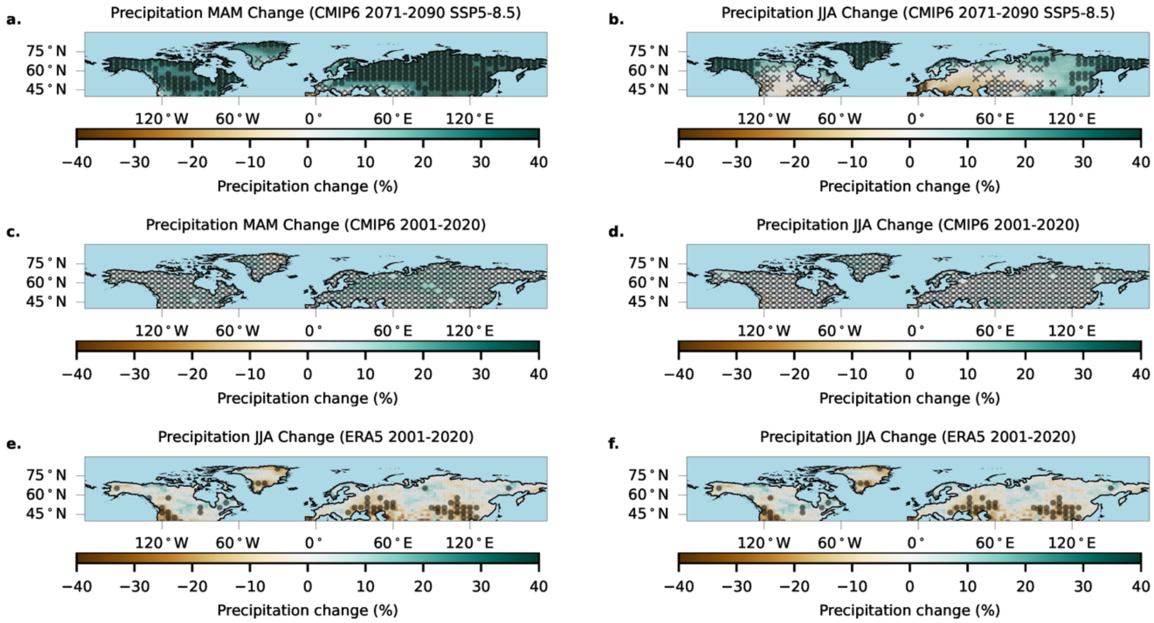

Extended data figure 7: As for Extended Data Figure 6 but showing precipitation

[Additional scenarios shown in Supplementary Information Figure S11]

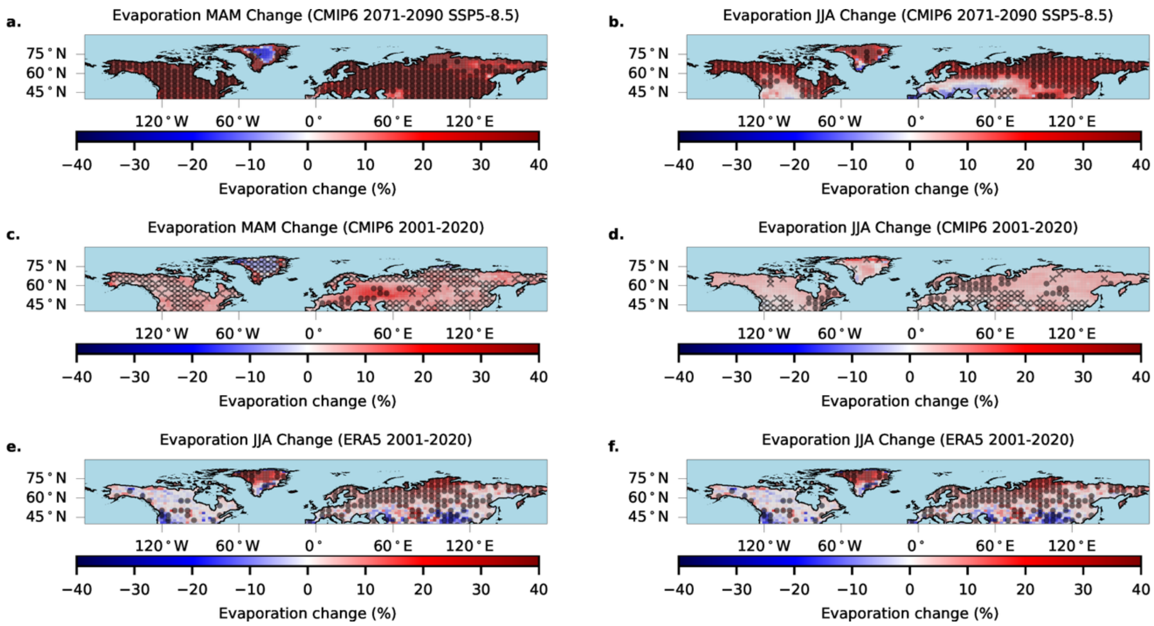

Extended data figure 8: As for Extended Data Figure 6 but showing total evapotranspiration

[Additional scenarios shown in Supplementary Information Figure S12]

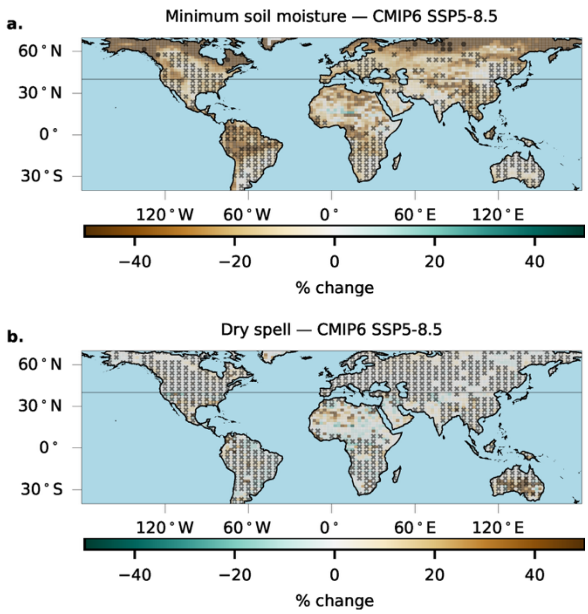

Extended data figure 9: Change in the character of drought through time, comparing 1940-2019 against 2020-2099: A) Minimum soil moisture during the season; B) Dry spell index (see methods for definition) [Additional scenarios shown in Supplementary Information Figures S13 and S14]

Supplementary Information

1.1. Supplementary Materials

Additional variables and seasons

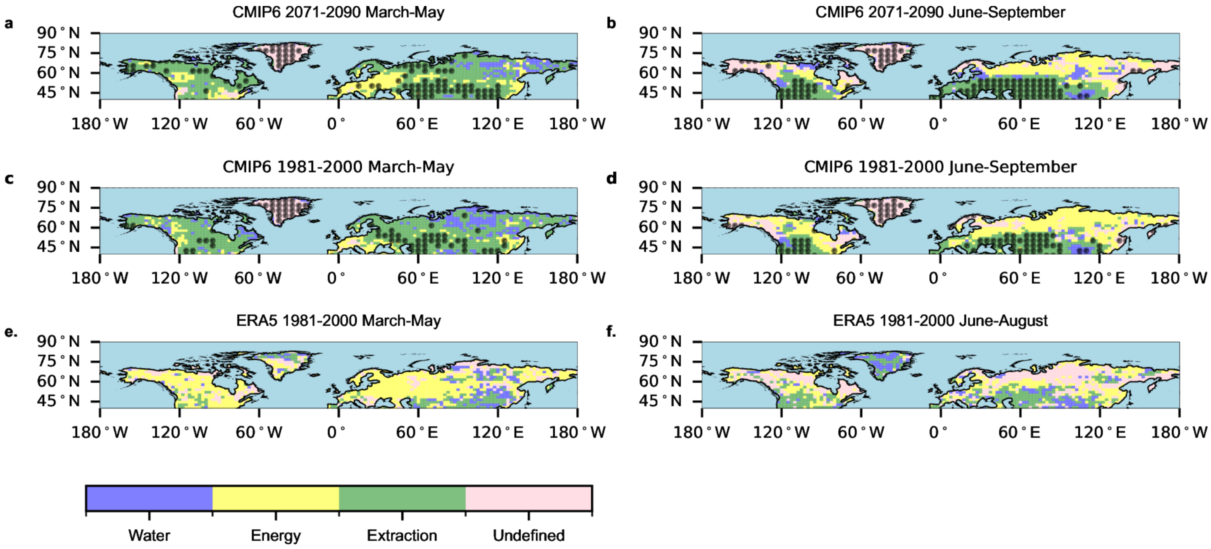

Figure S1: As for Figure 2 but showing the March-May and June-August calendar seasons

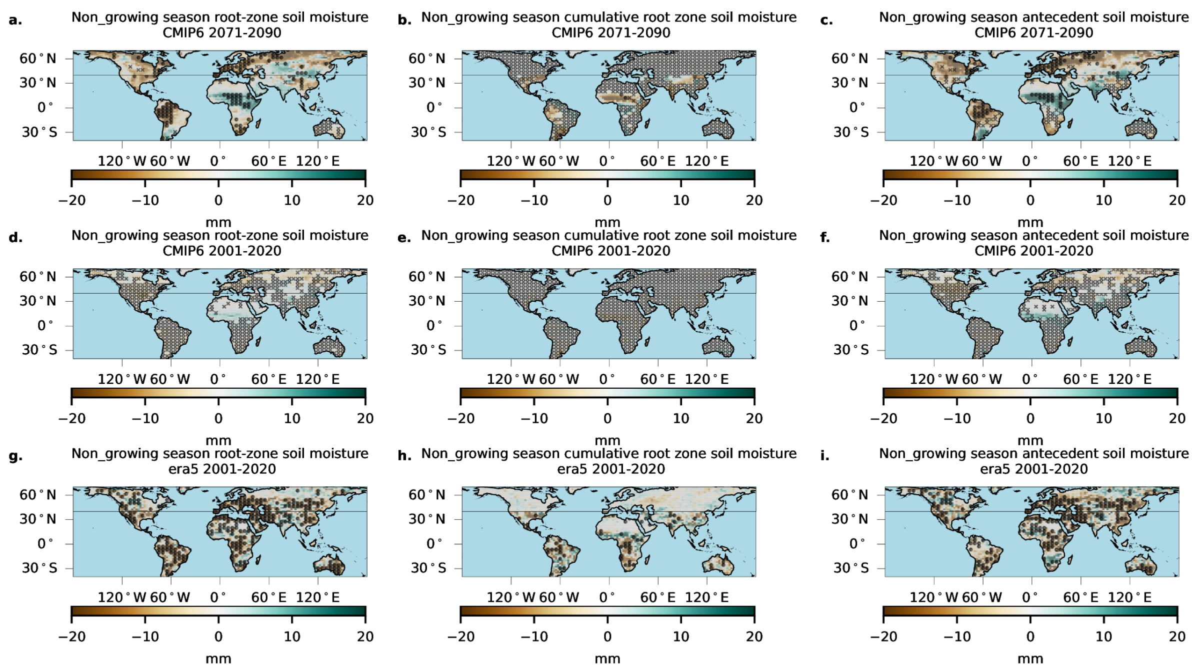

Figure S2: As for main paper Figure 4 but for the non-growing season

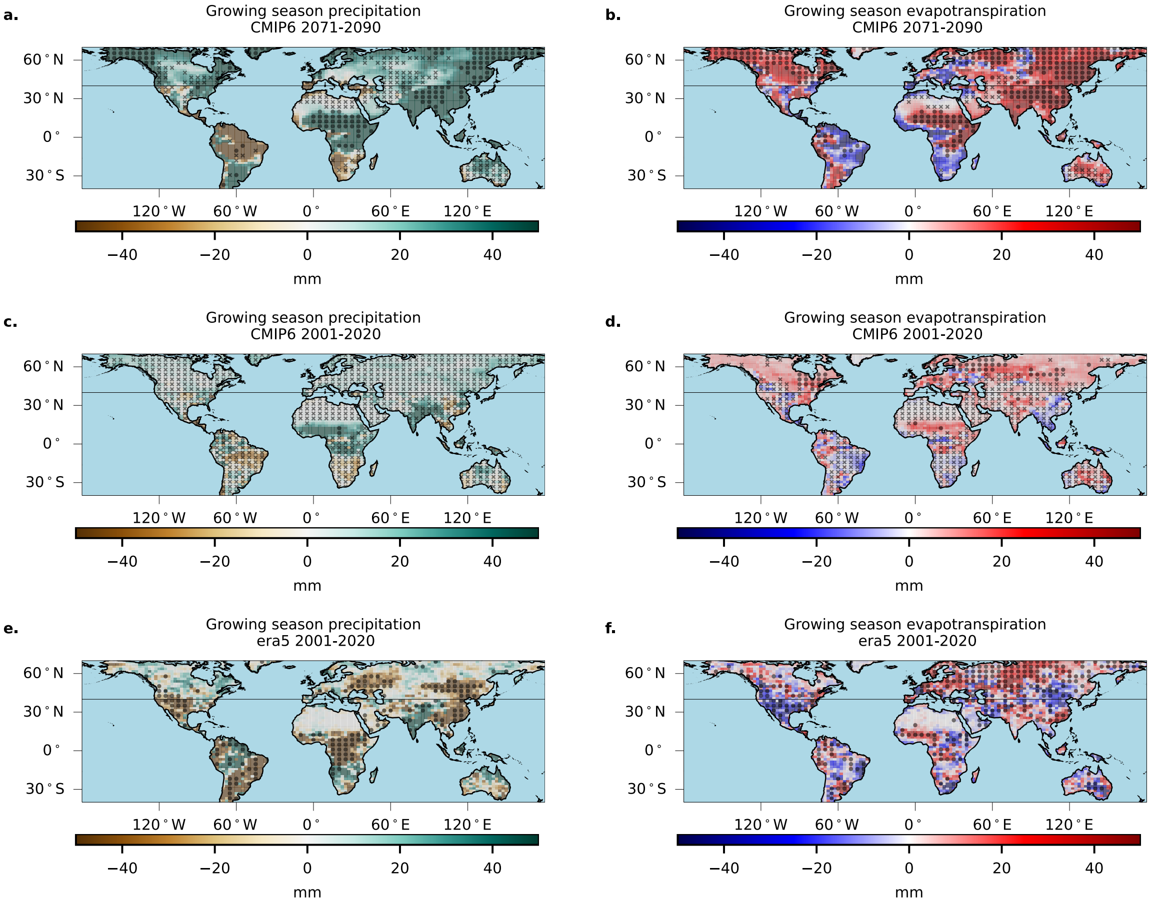

Figure S3: As for Figure 4a, d and g for growing season precipitation (panels a, c and e) and evapotranspiration (panels b, d and f)

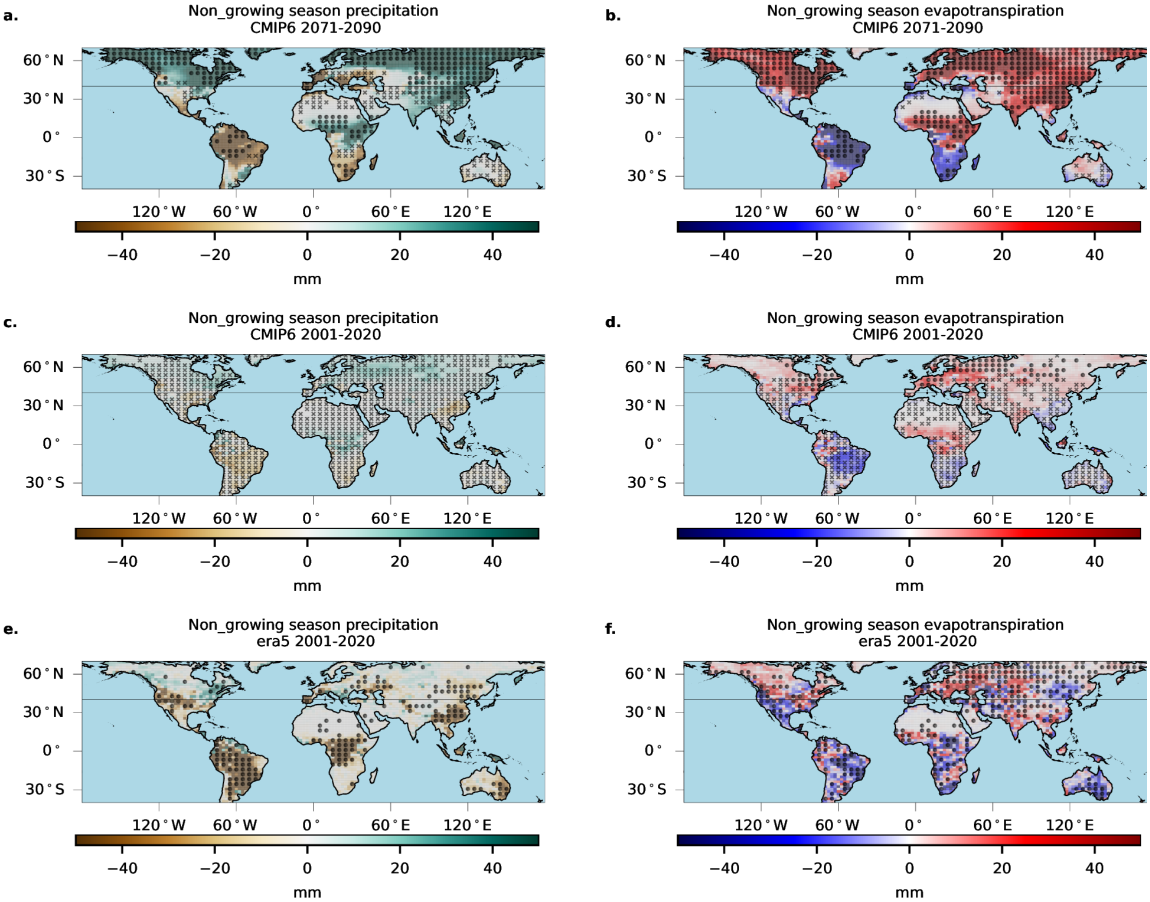

Figure S4: As for Figure S3 but for non-growing seasons.

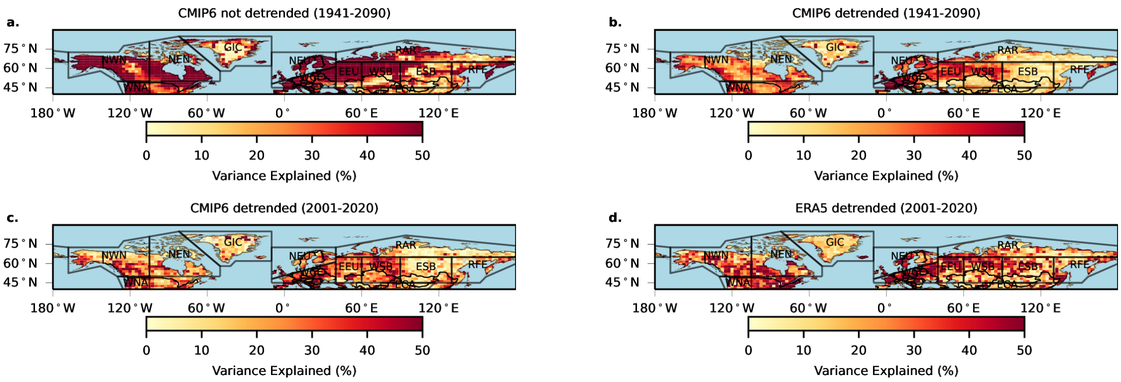

Figure S5: As for Extended Data Figure 5, but showing the variance in growing season soil moisture by explained by variability in cumulative soil moisture during the dominant season. Regions with a negative Pearson correlation coefficient between the two variables have been greyed out.

Addditional scenarios

Here we display projections for key variables and seasons for the SSP1-2.6, SSP2-4.5 and SSP3-7.0 and SSP5-8.5. Note that because fewer models include the required variables for the above SSPs than for SSP5-8.5, the following plots are based on a smaller multi-model ensemble (Table S1)

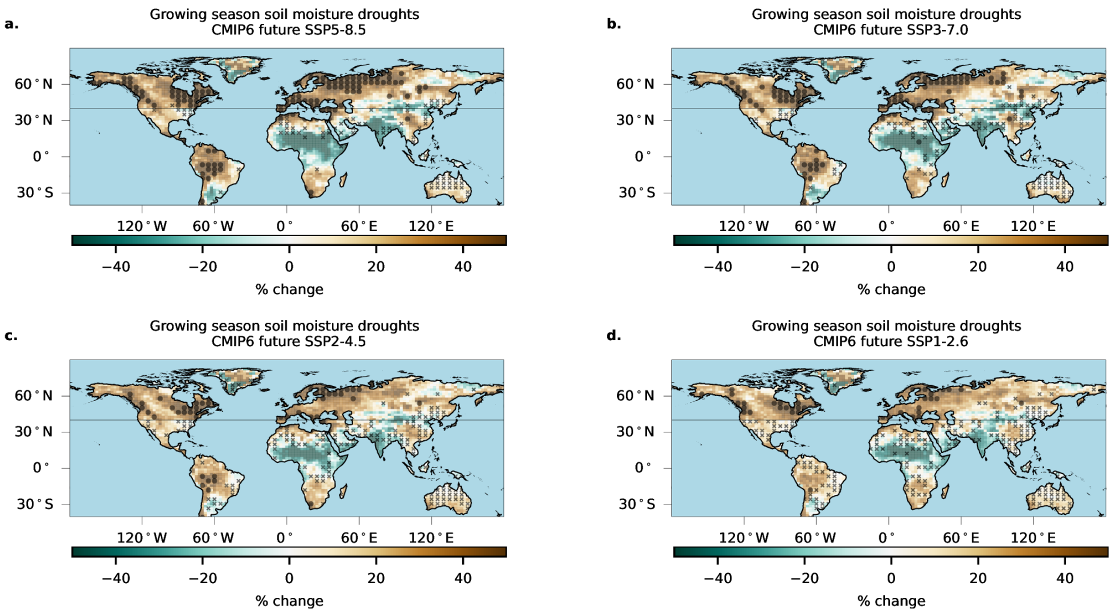

Figure S6: As for main paper Figure 4a but for SSP5-8.5, SSP3-7.0, SSP2-4.5 and SSP1-2.6

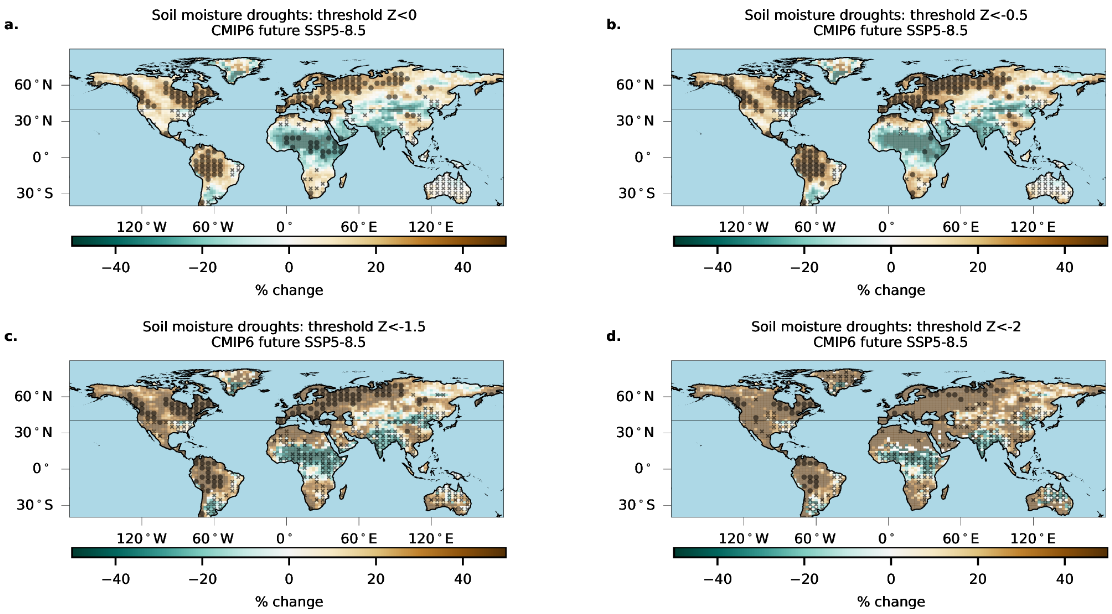

Figure S7: As for Figure 6B (which shows SSP5-8.5 only), comparing SSP5-8.5, SSP3-7.0, SSP2-4.5 and SSP1-2.6

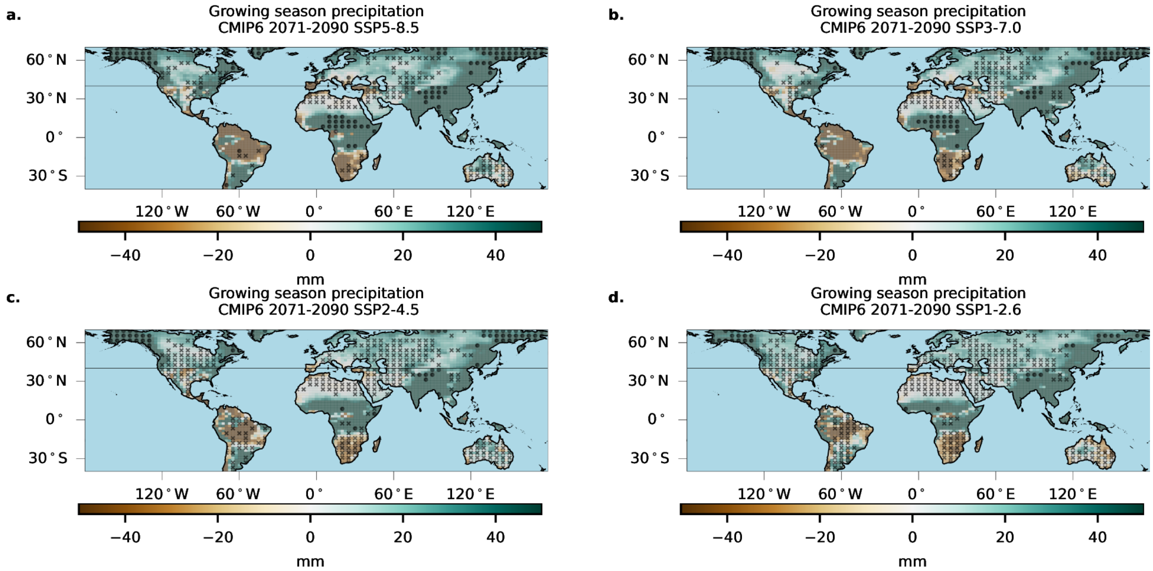

Figure S8: As for main paper Extended Data Figure 3A but for SSP5-8.5, SSP3-7.0, SSP2-4.5 and SSP1-2.6

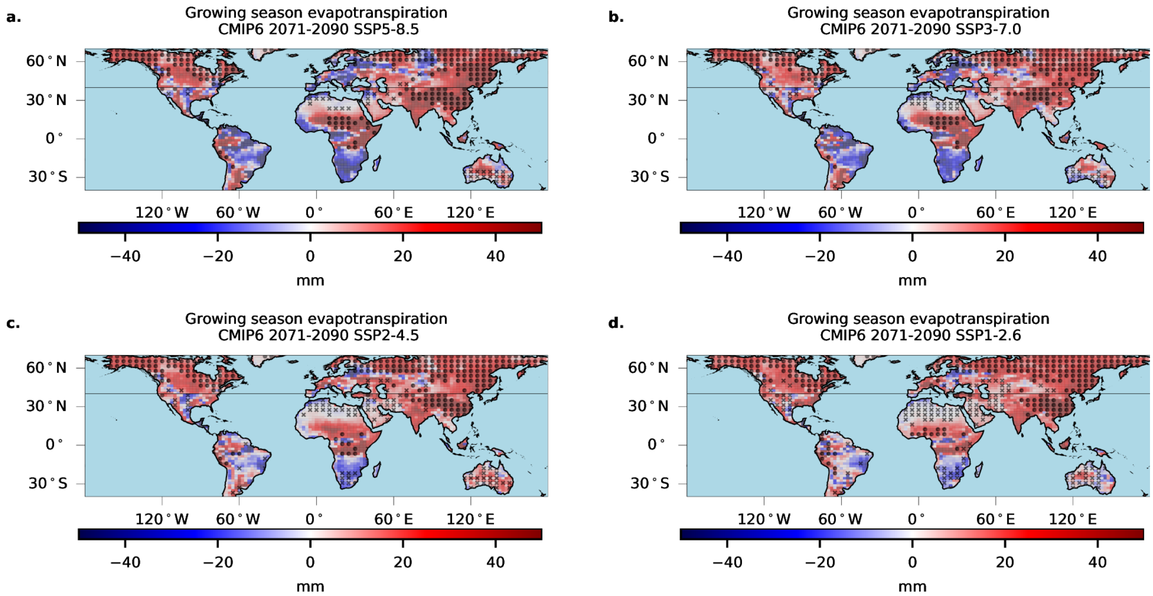

Figure S9: As for main paper Extended Data Figure 3B but for SSP5-8.5, SSP3-7.0, SSP2-4.5 and SSP1-2.6

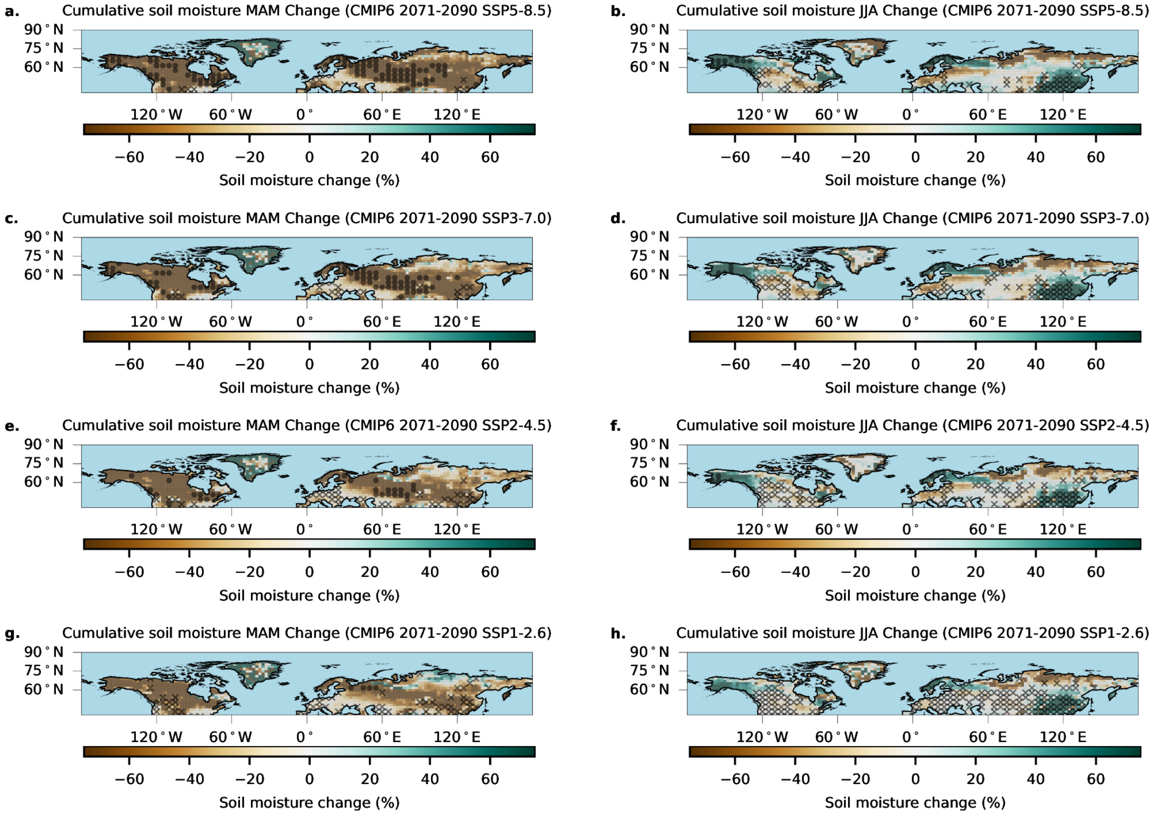

Figure S10: As for main paper Extended Data Figure 6A/B but for SSP5-8.5, SSP3-7.0, SSP2-4.5 and SSP1-2.6

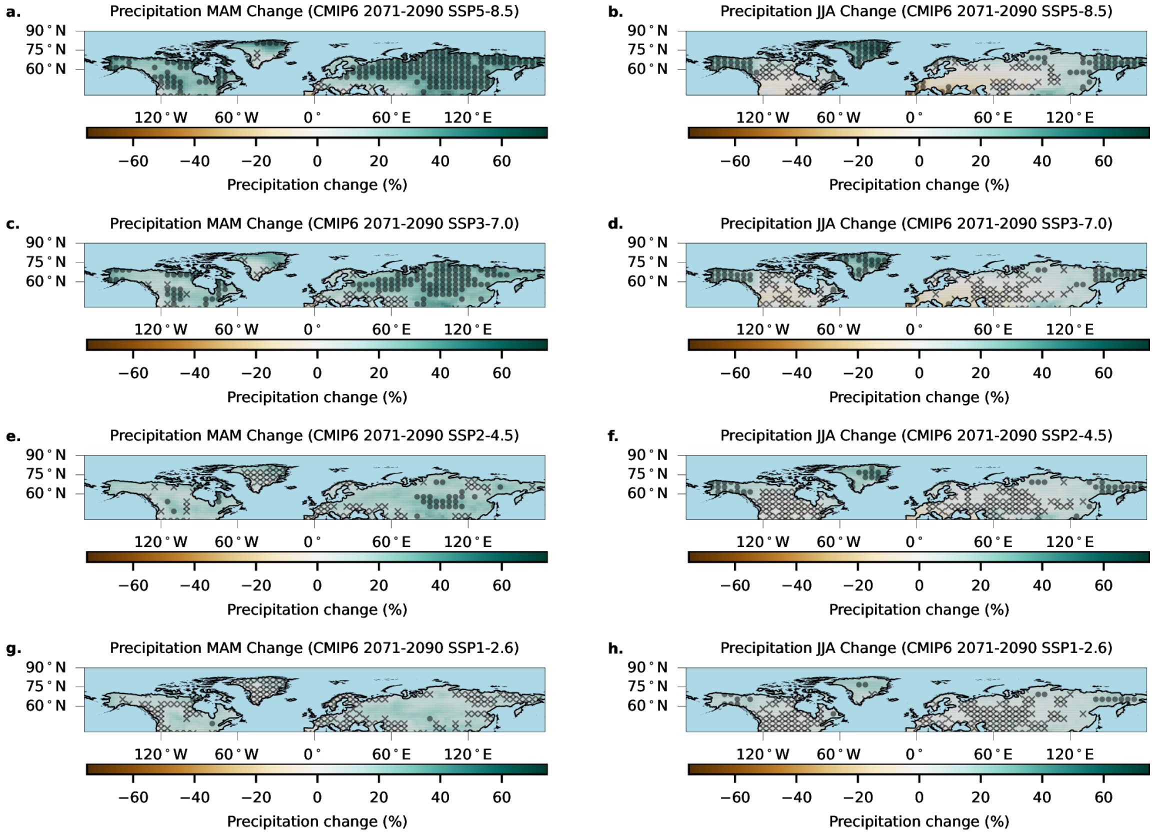

Figure S11: As for main paper Extended Data Figure 7A/B but for SSP5-8.5, SSP3-7.0, SSP2-4.5 and SSP1-2.6

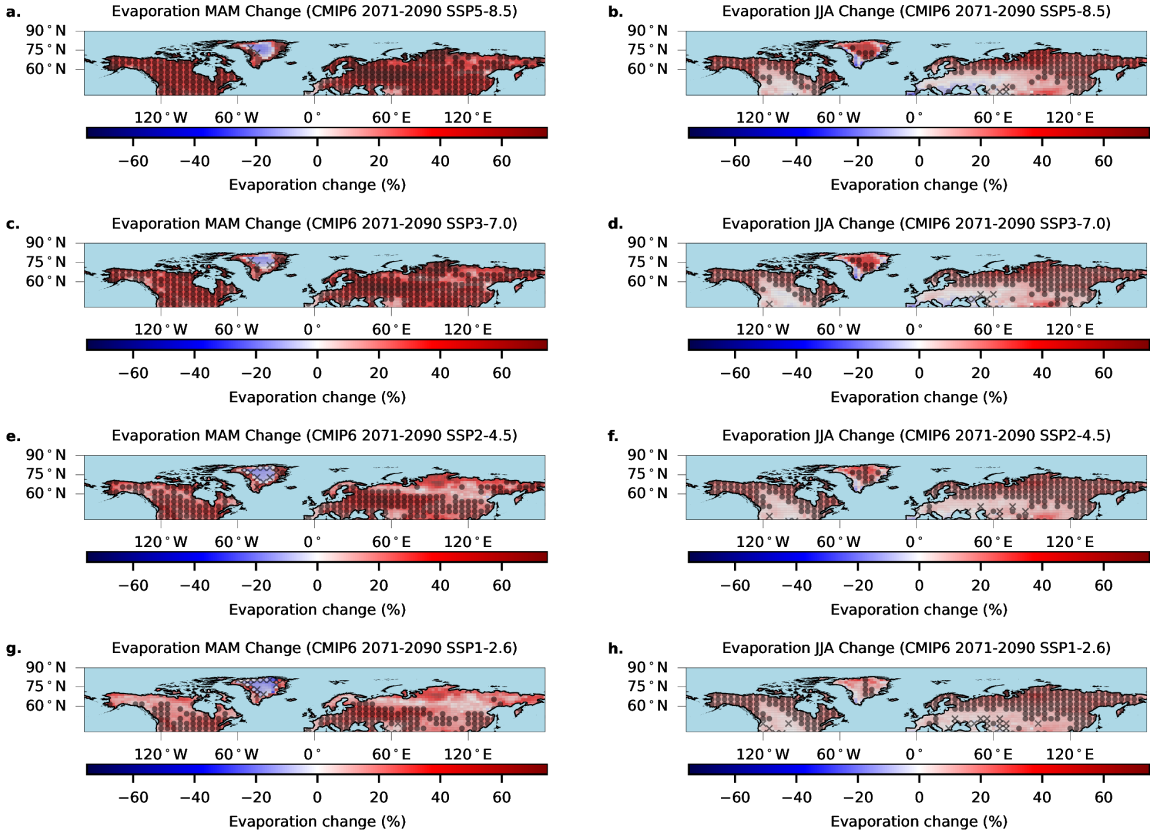

Figure S12: As for main paper Extended Data Figure 8A/B but for SSP5-8.5, SSP3-7.0, SSP2-4.5 and SSP1-2.6

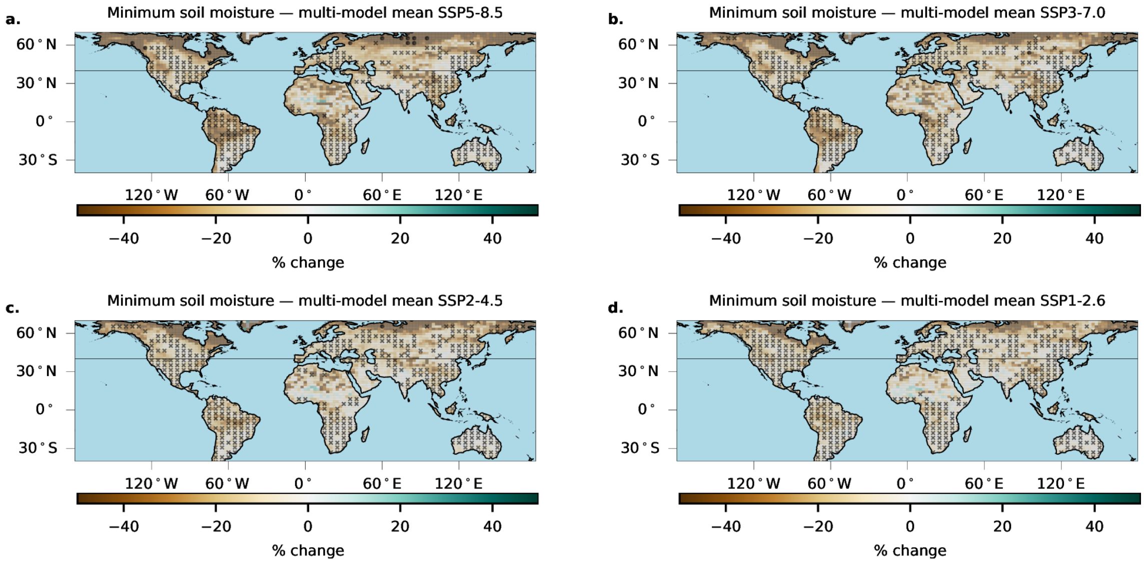

Figure S13: As for extended data Figure 9A but comparing SSP5-8.5, SSP3-7.0, SSP2-4.5 and SSP1-2.6

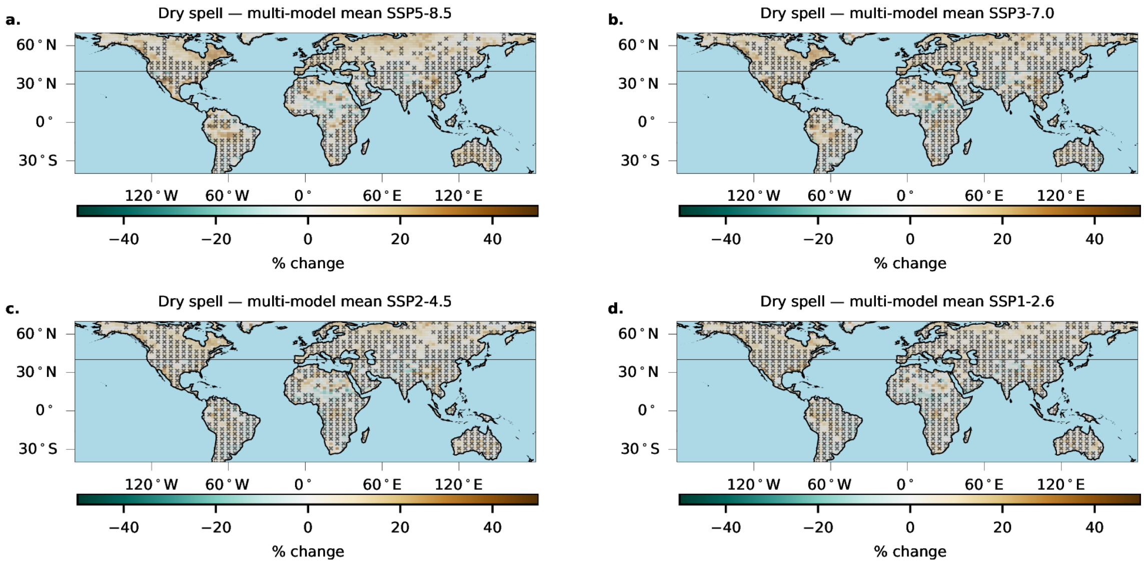

Figure S14: As for extended data Figure 9B but comparing SSP5-8.5, SSP3-7.0, SSP2-4.5 and SSP1-2.6

Further analyses of evaporative regimes

Surface and deep water control

In water-controlled seasons, evaporative fluxes are supply-limited: AET covaries with precipitation through surface wetness and/or root-zone replenishment, yielding a positive correlation between AET and SM, and weak or negative correlations between AET and shortwave radiation fluxes (SW). The positive AET–SM link can arise either indirectly (surface evaporation and interception track rainfall while SM is also set by rainfall) or directly (transpiration responds to root-zone soil moisture), but in both cases the diagnostic is precipitation supply limitation. It should be noted that the methodology used here does not allow us to distinguish between surface and deep water limitation because in both cases, soil moisture and AET are positively correlated.

In energy-controlled regimes, water is ample and AET rises with available energy. Higher AET thus coincides with greater soil-moisture drying, with soil moisture cumulation/drying driven by atmospheric demand. In extraction-controlled seasons, surface energy and near-surface water are generally sufficient such that **evaporation of near-surface and root zone water is not supply-limited;** variability in seasonal AET is instead dominated by **plant extraction capacity and canopy conductance** acting on root-zone moisture. Years with greater transpiration draw down soil moisture more strongly, so **AET and seasonal soil-moisture accumulation are negatively correlated.**

In both extraction-controlled and deep water-limited situations, seasonal soil moisture reflects the balance between precipitation inputs and transpiration losses. A negative AET–ΔSM correlation in extraction-controlled seasons typically occurs when soils begin the season sufficiently wet to support transpiration (above wilting), but in-season precipitation is too low to offset transpiration losses; soil moisture then declines toward a physiological threshold at which AET diminishes. Where water influx maintains soil moisture between critical and wilting points (deep water-limited), AET rises with soil moisture, producing a positive AET–ΔSM correlation and a damping of precipitation variability in ΔSM.

Geographical distribution of evaporative regimes

Figure 2 shows that, in the tropics, there is a tendency to transition from water-controlled during the growing season to extraction-controlled during the non-growing season because soil moisture accumulates during growing seasons and dries during non-growing seasons. In the extra-tropics, because soil moisture dries down during growing seasons and accumulates in non-growing seasons the opposite is true (Extended Data Figure 1D). The factors underpinning the spatial distribution of the energy-controlled regime also differ between the tropics and extra-tropics. In the highest latitudes, because solar radiation fluxes are low in comparison to the tropics, energy limitation dominates in both high and low precipitation climates in CMIP6 (Figure 2). In northernmost Eurasia, during the winter non-growing season, in ERA5, the evaporative regime cannot be defined. This may be because of the extra complexity introduced by snowmelt processes. In the tropics, the energy-controlled regime is found in wetter regions, simply because water is plentiful and vegetation is highly active – meaning that the only limiting factor left is solar energy. As a result, the energy-controlled regime is more widespread during the wet growing seasons, with only the wettest regions experiencing an energy-controlled regime year round.

Comparison between observed and modelled evaporative regimes

Comparison between Figure 2c/d and Figure 2e/f shows that, for the historical period, when data are aggregated into growing and non-growing seasons, models and reanalysis broadly agree on the distribution of regimes in both the tropics and extra-tropics – giving us confidence in model projections of future changes in the spatial and seasonal distribution of the regimes. Figure 2A and B show that in the tropics, these projected changes are minor. In the extra-tropics, in contrast, there are significant changes projected over the 21st Century, with the most marked change being increased latitudinal extent of the water-controlled regime - consistent with the projected extension of sub-tropical arid zones under climate change[1].

<u>Effect of evaporative regime on consistency in model projections of cumulated soil moisture over the northern hemisphere extra-tropics</u>

To test whether projections of cumulated soil-moisture change are more robust in demand-limited (extraction/energy) than in supply-limited (water) regimes, we conducted a regime- and season-specific intermodel sensitivity analysis. For each model, we selected grid cells by regime from the seasonal regime map (tropics: wet; extratropics: summer), computed seasonal means of cumulated soil moisture for 1981–2000 and 2071–2090, and formed a guarded percent change (with an absolute-change fallback where historical baselines were too small for percent change to be meaningful). We then calculated land-only, area-weighted regional means by regime and summarized intermodel behavior using the SNR = |mean|/SD to characterise ensemble agreement. Preliminary analyses suggest that the extratropics (summer), extraction- and energy-controlled areas show greater consistency than water-controlled regimes (SNR = 1.35 and 0.44 compared to SNR = 0.24).

1.2. Supplementary materials for the methods section

Models and data

Supplementary Table 1: A few details of the models and reanalysis used in this study. Models highlighted in red had all data for all four SSPs

Model /Reanalysis	Land-surface model	Number of layers	Soil depth (m)	Approximate horizontal resolution (degrees)
ERA5	HTESSEL	4	1.9	0.75x0.75
UKESM1-0-LL	JULES	4	2	1.875x1.25
CAS-ESM2-0	CoLM	15	42.1	1.4x1.4
CanESM5	CLASS	3	4.1	2.8x2.8
CMCC-CM2-SR5	CLM4.5	20	0.4 - 8.5	1x1
CMCC-ESM2	CLM4.5	20	0.4 - 8.5	1x1
CNRM-CM6-1	ISBA-CTRIP	14	12	1x1
ACCESS-ESM1-5	CABLE2.4	6	2.9	1.25x1.875
ACCESS-CM2	CABLE 2.4	6	2.9	1.25x1.875
EC-Earth3	HTESSEL	4	1.9	0.4x0.4
EC-Earth3-CC	HTESSEL	4	1.9	0.4x0.4
IPSL-CM6A-LR	ORCHIDEE	18	65.6	3.75x0.95
MIROC6	MATSIRO6.0	6	9	1.4x1.4
MPI-ESM1-2-LR	JSBACH3.20	5	7	2.5x2.5
CESM2-WACCM	CLM5	25	42	1x1

NorESM2-LM	CLM5	25	42	2x2
GFDL-ESM4	GFDL-LM4.0.1	20	8.8	1x1
HadGEM3- LL	JULES	4	2	1.875x1.25

Identification of growing seasons

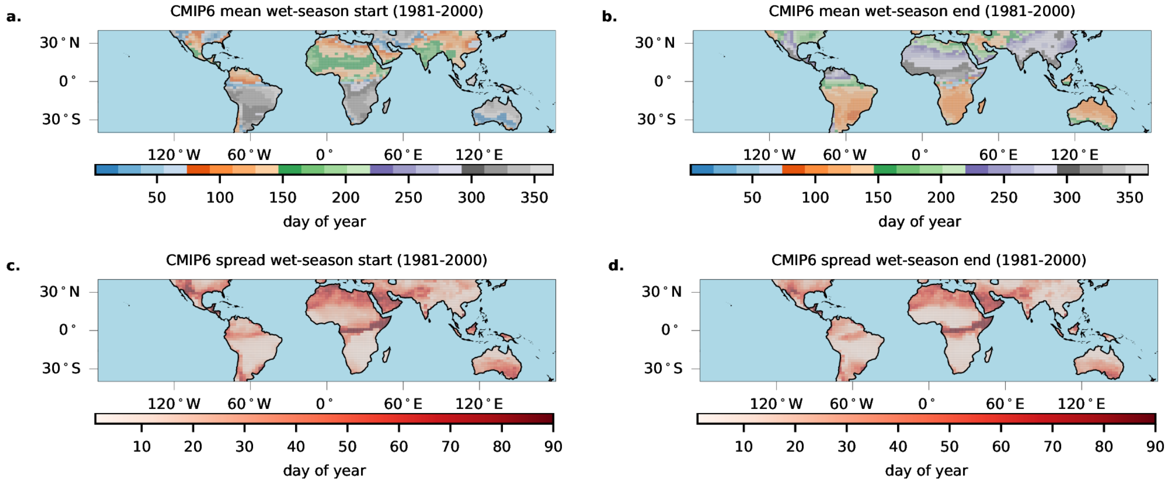

Figure S15: Objective diagnosis of rainy seasons for the CMIP6 multi-model ensemble within the tropics/sub-tropics (40S-40N). A) Season start; B) Season end; C) Intra-model standard deviation for the season start; C) Intra-model standard deviation for the season end

Further details of the statistical testing

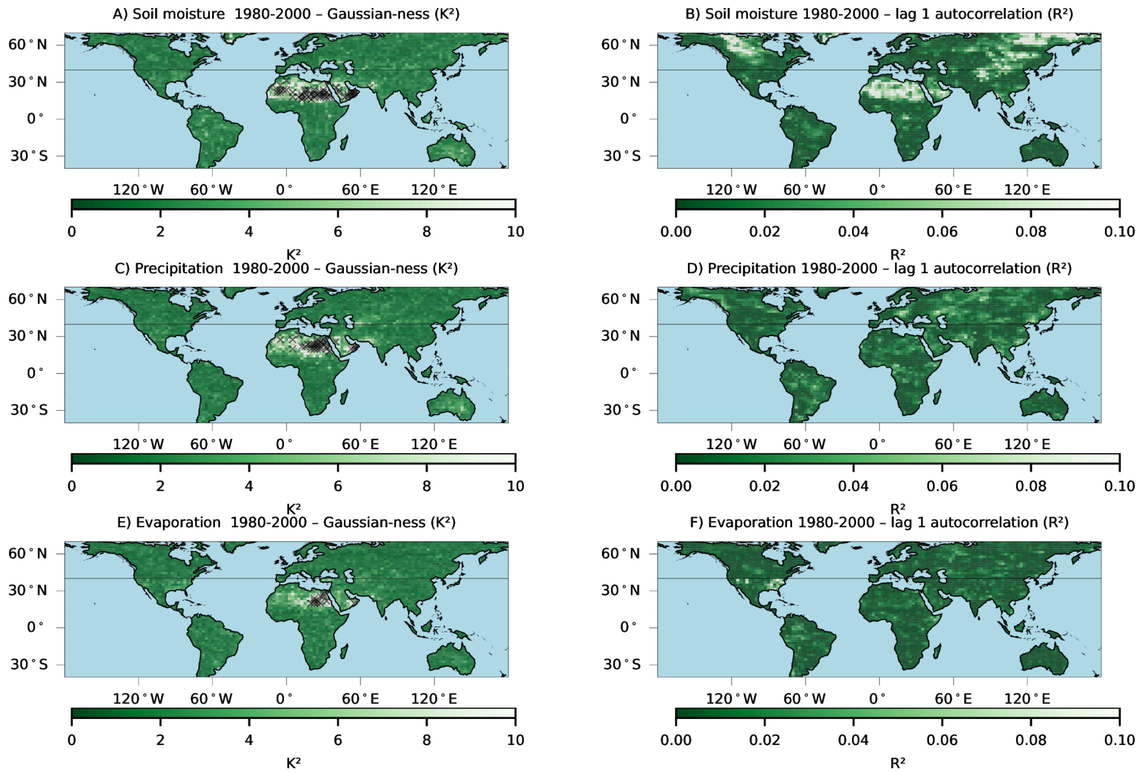

Figure S16: Assumption diagnostics. Panels A, C, and E map D'Agostino–Pearson K^2 for AR(1)-whitened residuals of growing season soil moisture, precipitation and evaporation (1980–2000); lower $K^2 \approx$ more Gaussian. Panels B, D, F show lag-1 autocorrelation of the corresponding detrended series. Markers denote grid cells where >67% of models reject normality at the 5% level (two-sided K^2), i.e., consensus non-Gaussianity. Panels B, D, and F map lag-1 autocorrelation of the corresponding detrended annual/seasonal series. For all panels, shading denotes the CMIP6 multi-model mean diagnostic.

1 Scheff, J. & Frierson, D. M. Terrestrial aridity and its response to greenhouse warming across CMIP5 climate models. *Journal of Climate* **28**, 5583-5600 (2015).